Tuning the FoCal prototype detector with cosmic muons

28th December, 2013

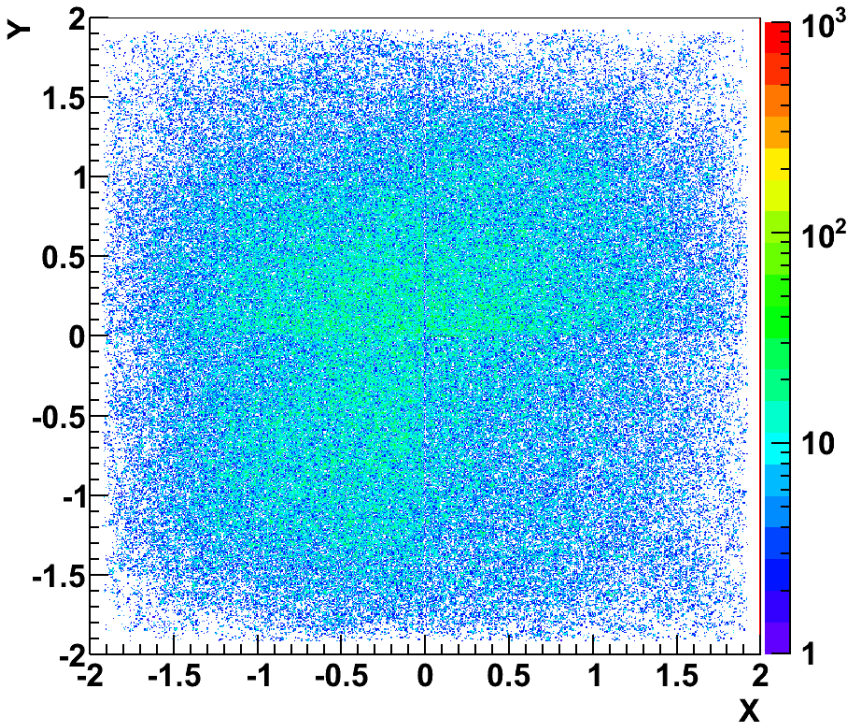

Author:
Nikkie Deelen
Student Number: 3469840

Supervisors:
Physics
Dr. ir. G.J.L Nooren
Chemistry
Prof. dr. A. Meijerink

Universiteit Utrecht

Abstract

This thesis is on the research of tuning the Foward Calorimeter (FoCal) prototype detector with cosmic muons. First the performance of the prototype detector was investigated. An important result was that the detector prototype response was stable in time. In order to estimate the detector performance, the amount of lost triggers and lost tracks were investigated too. During this study it was found that (3 ± 2) % of the triggers was lost during a measurement and that (50 ± 3) % of the tracks was lost with the present version of the software (code13052013). An understanding of what is causing this problem has not yet been reached.

The second part of the investigation was meant to come to an understanding of how the chips in the detector can be tuned using cosmic muons. For this purpose, one of the chip parameters was changed (*P1*) and the results were analysed. It was found that some of the chips were already operating with good *P1* settings but for other chips better settings were obtained. There were also some patterns discovered of how the *P1* chip settings relate to results of a measurement.

Contents

Chapter 1

Introduction

During this bachelor research, different aspects of the Foward Calorimeter (FoCal) prototype detector are investigated. The prototype is meant to test the possibilities for the FoCal detector being a part of an upgrade of the "A Large Ion Collider Experiment" detector (ALICE) at CERN. It is a digital electromagnetic sampling calorimeter that measures particles in the forward beam direction of CERN's Large Hadron Collider (LHC).

In the second chapter, cosmic radiation, the interaction of radiation with matter and the detector principles used during this research are introduced. The FoCal prototype, its experimental setup, the data acquisition and analysis are explained in chapter 3. Subsequently there are two chapters devoted to the characterisation of the FoCal prototype; one on the detector performance which contains the investigation of the time stability of the detector and the lost triggers and tracks and one on chip characterisation. The report is concluded by summarizing the results and by providing the perspectives on a possible future research.

Chapter 2

Theory

In this chapter, a summary of the theory connected to the research is given. First it is explained how cosmic radiation reaches the surface of the Earth. This is because cosmic muons were used to characterise the FoCal detector prototype. Then electromagnetic interactions between particles and matter are explained, which is necessary to understand FoCal detector principle. At last electromagnetic calorimeters, scintillation counters, silicon detectors and FoCal physics motivations are described in order to form a complete picture of the subject of this thesis.

2.1 Cosmic radiation

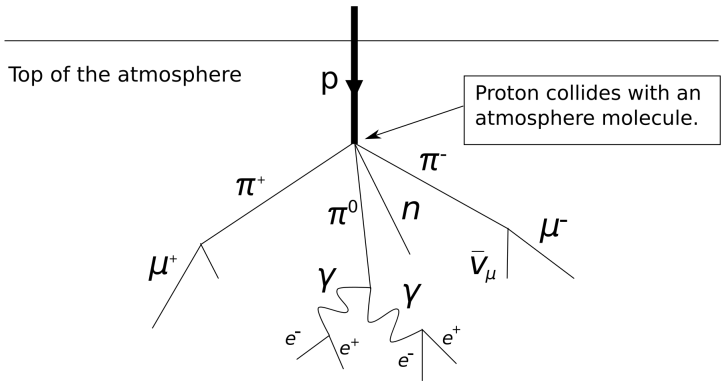

Figure 2.1: A proton producing a cascade of particles in the atmosphere [1]

When cosmic rays, mostly protons, enter the atmosphere of the Earth, they interact with nuclei producing a cascade of secondary particles [4]. These secondary particles are mainly pions, kaons and nucleons. The neutral pions in this cascade immediately decay into two photons because of their short lifetime ($\tau = 8.4 \cdot 10^{-17}$ s). These photons can undergo pair production if they have enough energy. The charged pions ($\tau = 2.6 \cdot 10^{-8}$ s) interact further with the air molecules until they decay into muons and neutrinos. A schematic view of a cascade in the Earth's atmosphere is given in Fig. 2.1. The muons have high velocity and hence relativistic effects play a role. Despite their lifetime of $\tau = 2.2 \cdot 10^{-6}$ s muons can reach the surface of the Earth because of time dilation. Take for instance muons with an energy of 2 GeV. The relativistic energy of a particle is given in the equation below.

$$E = \sqrt{(mc^2)^2 + (pc)^2} \tag{2.1}$$

With this formula the velocity of the muon can be calculated from the momentum, p, which is the product of mass and velocity. Then the time dilation experienced by a muon can be computed with

$$t = \gamma \cdot t' \tag{2.2}$$

where γ is the Lorentz factor. Thus a muon with an energy of 2 GeV can travel for 13.8 km before decaying into an electron and a neutrino.

2.2 Electromagnetic interactions

Particle detection happens via interactions with the detector material [5]. Electromagnetic interactions are based on energy transfer between the incoming particle and the material. The energy transfer can be observed in several ways, for instance through ionized atoms or Čerenkov radiation in the detector. Different particles interact with the detector material in different ways. Heavy charged particles lose their energy mostly via Coulomb interactions in collisions with the electrons bound to the detector material's atoms. Light charged particles lose energy via Coulomb interactions as well as radiation and have to be treated differently because of that. Photons can transfer their energy through either one of three different effects; the photoelectric effect, the Compton effect or pair production.

Then there is another aspect of electromagnetic interactions which is important for the subject of this report. When high energetic particles enter a detector they can cause electromagnetic showers. This phenomenon will be explained in this section as well.

2.2.1 Heavy charged particles

When a heavy charged particle collides with an atomic electron, the electron can be excited into a higher energy state or it can be ejected from the atom which is called ionisation [8]. Because of this collision, the incoming particle loses energy. The amount of energy lost by the particle is given by the Bethe-Bloch formula [3]. This formula gives a quantum mechanical description of the mean energy loss per travelled distance x in $\mathrm{g\,cm^{-1}}$. The Bethe-Bloch formula is given by

$$-\left\langle \frac{dE}{dx} \right\rangle = 4\pi N_A r_e^2 m_e c^2 z^2 \frac{Z}{A} \frac{1}{\beta^2} \left[\frac{1}{2} ln \frac{2m_e c^2 \beta^2 \gamma^2 T_{max}}{I^2} - \beta^2 - \frac{\delta(\beta\gamma)}{2} \right] \tag{2.3}$$

where N_A is Avogadro's number, r_e is the classical electron radius $\frac{e^2}{4\pi\epsilon_0 m_e c^2}$, m_e is the electron mass, c is the speed of light, z is the charge of the particle, Z and A are the atomic number and mass of the detector medium, β is the v/c with v the particles velocity, γ is the Lorentz factor $\frac{1}{\sqrt{1-\beta^2}}$, T_{max} is the maximum transferable kinetic energy, I an ionisation potential and $\delta(\gamma\beta)$ is the correction to the density effect in ionization energy loss.

The maximum amount of kinetic energy a particle can lose during a single collision (T_{max}) is given by:

$$T_{max} = \frac{2m_e c^2 \beta^2 \gamma^2}{1 + 2\gamma m_e/M + (m_e/M)^2} \tag{2.4}$$

where M is the mass of the incoming particle. For muons the mean energy loss per unit of momentum is depicted in Fig. 2.2. Here it is shown that at a certain momentum (p_m) a minimum in energy loss occurs. If a particle has a momentum which is lower than this p_m, its energy loss is proportional to $1/v^2$. Therefore the energy loss of a non-relativistic particle increases when it slows down in a material. Above the p_m the energy loss increases much more slowly.

When a particle traverses thin layers of material, statistical fluctuations on the energy loss of a charged particle can be described by the Landau distribution which is shown in Fig. 2.3. [3].

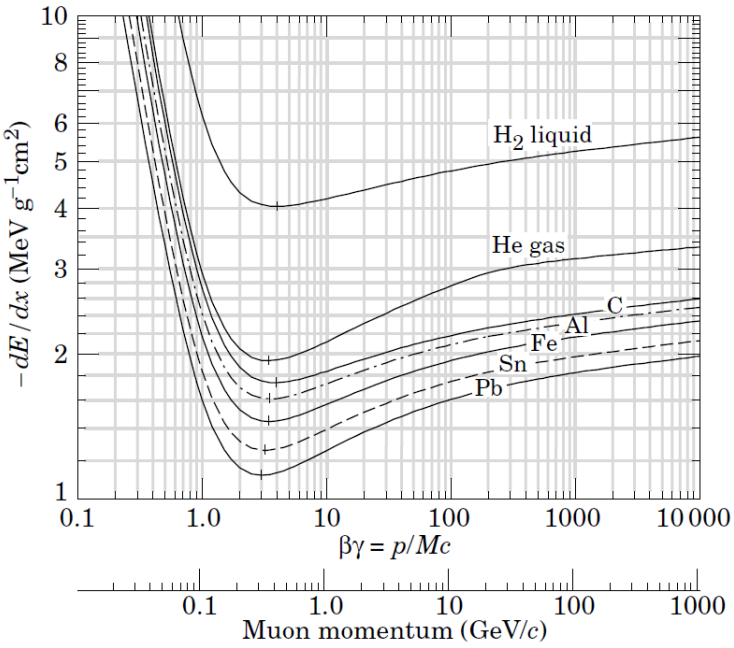

Figure 2.2: The energy loss for muons in different materials [3].

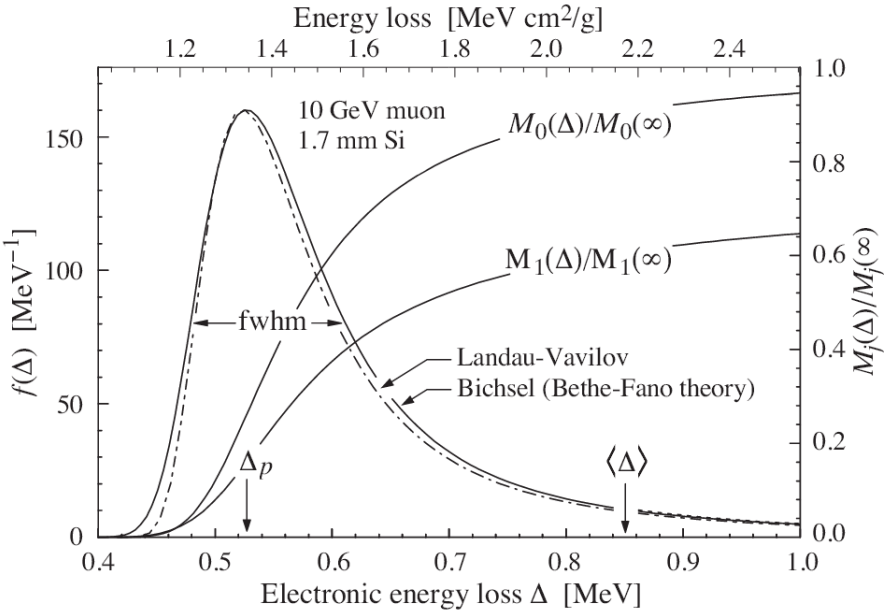

Figure 2.3: The Landau distribution for a 10 GeV muon (dot-dashed line) traversing 1.7 mm silicon [3].

$$\delta_p = \xi \left[ln\frac{2m_e c^2\beta^2\gamma^2}{I} + ln\frac{\xi}{I} + j^2 - \beta^2 - \delta(\beta\gamma) \right] \tag{2.5}$$

$$\xi = 2\pi N_A r_e^2 m_e c^2 \frac{Z}{A}\frac{x}{\beta^2} \tag{2.6}$$

$$j \in \mathbb{R}_+ \tag{2.7}$$

The most probable energy loss is given by Eq. 2.5 for a detector with thickness x and $j = 0.200$ in $\mathrm{g\,cm^{-1}}$. The Landau distribution can be used under the assumptions that:

- The maximum transferable energy is infinite
- The velocity of the incoming particle remains almost the same after hitting a thin material
- The electron involved in the collision is treated as free since the electron binding energy in a collision is negligible.

2.2.2 Light charged particles - electrons

The energy loss of electrons in matter differs from that of heavy particles mostly because these light particles can also lose energy via radiation. There is a well defined critical energy, E_c, for which electrons with greater energy lose their energy mostly through radiation. For solids, this critical energy is roughly given by $E_c \approx \frac{610\,\mathrm{MeV}}{Z+1.24}$, with Z the atomic number of the absorber material. For gases the critical energy is given by $E_c \approx \frac{710\,\mathrm{MeV}}{Z+0.92}$. The energy loss through radiation is caused by the electron being deflected in the Coulomb field of the nuclei of the detector material and it is called Bremsstrahlung.

2.2.3 Photons

If a photon goes through matter, an interaction can take place in three different ways. These are the photoelectric effect, the Compton effect and pair production [5]. For an exact treatment of these three processes one needs the tools of quantum electrodynamics that will not be included in this report. Instead a description of the three effects is given.

A photon traversing matter can be absorbed by an atom. When this happens and an electron is ejected from the atom (ionization) the photoelectric effect occurs. The electron can be ejected because the energy of the incoming photon is converted into kinetic energy of the electron.

When a photon scatters from an free electron it is called the Compton effect. Through this, the photon loses energy and its wavelength increases.

In matter, when the photon has enough energy ($E \geq 2m_e c^2$), pair production can occur. In this process the photon is converted in an electron-positron pair. This can only happen in the Coulomb field of the nucleus, otherwise energy and momentum cannot be conserved.

Each one of these effects is dominant at a different energy regime. The photoelectric effect dominates below $\sim 500\,\mathrm{keV}$, the Compton effect between $\sim 800\,\mathrm{keV}$ and $3\,\mathrm{MeV}$ and pair production is dominant above $10\,\mathrm{MeV}$.

2.2.4 Electromagnetic showers

When the Bremsstrahlung-photons have enough energy ($E \geq 2m_e c^2$) they can be converted into an electron and a positron [5]. These particles can also be deflected by the Coulomb field of the nuclei in the material causing Bremsstrahlung radiation again. This process stops when the photons do not have enough energy to cause pair production anymore. The so obtained cascade is called a shower. An incoming electron can start a shower as well as an incoming photon.

2.3 Detectors

2.3.1 Electromagnetic calorimeters

Calorimeters are designed to measure the energy of particles [4]. This occurs by the absorption of the energy of the particle by the detector material. The measurement performed by a calorimeter is considered destructive because the entire energy of the particle is absorbed. Electromagnetic calorimeters are designed to measure the energy of charged particles like electrons or positrons. When these particles produce a shower in the detector material, the amount of released photons is a measure for the energy of the particle.

Calorimeters use materials with a high Z-value (atomic number) to maximise the energy absorption probability due to the high electron density. A widely used material for electromagnetic calorimeters is lead with a Z-value of 82.

There are two sorts of electromagnetic calorimeters, the homogeneous calorimeters and the sampling calorimeters. In a homogeneous calorimeter, the detector consists of one material in which the particles energy is absorbed and in which the signal is generated too. In a sampling calorimeter the energy deposition (passive medium) and the signal generation (active medium) are separated in different materials. This can be done by separating the passive medium and the active medium in different layers. But it is also common to have one piece of material in which different sorts of molecules are incorporated where one sort absorbs the energy and the other generates the signal.

One can also make the distinction between analogue and digital electromagnetic calorimeters. In digital electromagnetic calorimeters the signals are counted in well-defined units. Therefore the signal can only have a discreet value. On the contrary in analogue electromagnetic calorimeters the signal can have any value, it is not restricted to predetermined unit values.

2.3.2 Scintillation counters

Scintillation counters are detectors in which the energy deposited by the incoming particle is converted into light [4]. This light is converted to an electrical signal and amplified by a photomultiplier tube. A schematic drawing of a scintillation counter is shown in Fig. 2.4.

In scintillating material fluorescence occurs due to de-excitation of the material that is ionised by a traversing particle. The energy deposition is already explained in Sections 2.2.1 and 2.2.2. Scintillation materials could be of any type, from solid crystals to plastics. The most common used plastic materials are aromatic plastic bases. The aromatic rings in these plastics are responsible for their fluorescent properties.

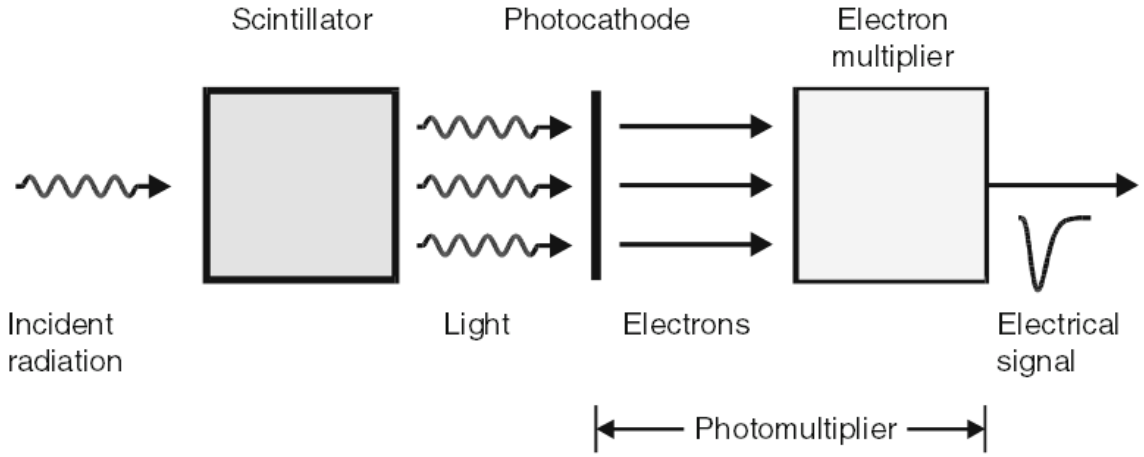

Figure 2.4: Schematic drawing of a scintillation counter [4].

2.3.3 Silicon detectors

Silicon detectors are a type of semiconductor detectors which are used to detect charged particles [9]. The charged particles traversing the detector produce electron-hole pairs. The drifting of these mobile charges causes charge to flow towards an external circuit where the signal is produced.

In the FoCal prototype, so-called Monolithic Active Pixel Sensors (MAPS) are used which are a type of silicon detectors. MAPS consist of different layers with different doping levels namely the p++ layer, the p-epitaxial layer and the p+ layer. The charge collecting element in this system is a n-well; because of their high doping level, the p++ and p+ layers act as mirrors causing the electrons to flow in the direction of the n-well. The holes flow in the opposite direction. A schematic drawing of a MAPS pixel is shown in Fig. 2.5.

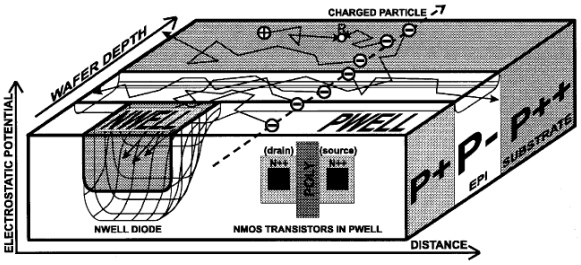

Figure 2.5: A schematic drawing of the internal structure of a MAPS pixel. A charged particle traversing the pixel produces mobile charges which drift in every direction. The large difference in doping level between the epitaxial layer and the p++- and p+ layer causes the charges to flow to the n-type well [9].

2.3.4 Forward Calorimeter (FoCal)

The FoCal detector is a proposed upgrade detector and it is an electromagnetic calorimeter that is designed to measure the energy of particles in the forward beam direction of CERN's LHC [2]. The FoCal prototype is a digital electromagnetic sampling calorimeter and it consists of tungsten layers for the energy deposition alternated with silicon layers (MAPS chips) for signal generation.

The main feature of FoCal is that this detector should be able to reconstruct π^0 decays (Eq. (2.8)) at very small opening angles, meaning that the angle between the two photons of the π^0 decay is very small. In this manner, FoCal is able to resolve between photons which come from the quark-gluon plasma (QGP) investigated in ALICE (A Large Ion Collider Experiment) and the π^0 photons.

$$\pi^0 \longrightarrow \gamma + \gamma \tag{2.8}$$

The QGP is a very dense state of matter with a very high temperature (100,000 times the sun's core temperature) [7]. It is a plasma of deconfined quarks and gluons and it is believed that this was the state the universe 10μs after the Big Bang.

Chapter 3

The FoCal prototype detector and data collection and analysis

During all the measurements reported in this thesis the same experimental setup was used. This setup and the methods for taking and analyzing data are described and explained in this chapter as well.

3.1 Experimental setup

3.1.1 The FoCal prototype detector

Fig. 3.1 shows a picture and a drawing of the FoCal prototype detector. The detector is marked with the blue box and it is positioned behind all the small cables on the right in the picture. The detector consists of twenty-four layers of absorber material alternated with the silicon sensor planes. Each layer is build up of two modules. Each module contains two chips that are placed next to each other on a tungsten plate. The chips used in the prototype detector are MAPS chips (see Section 2.3.3) for a total of 96 chips in the whole detector. A schematic drawing of a layer of four chips (two modules) is shown in Fig. 3.2. In each layer, two of the four chips have their upper side facing up and the other two have their upper side facing down. A particle traversing the chip deposes energy and a consequent electrical signal will be generated.

In the FoCal setup the two scintillator plus PMT (PhotoMultiplier Tube) systems are located above and below the detector and they are denoted as Back PMT and Front PMT respectively. The magenta boxes indicate where the scintillation material is placed. In both scintillators, this material is a $40 \times 40 \times 10\,\mathrm{mm}^3$ piece of NE104 POPOP plastic (1,4-bis-[2-(5-phenyloxazolyl)]-benzene). In this material a light pulse is generated whenever a muon traverses it. The signals of both scintillators are sent to a signal registration system that checks whether two signals fall together in a time window of 100 ns. When this occurs it is called trigger.

The small cables in front of the detector (see Fig. 3.1) transport the data coming from the chips to the printed circuit boards (PCB's, green box). These are connected to Bergen boxes (not in the picture) with the thick cables on the left. Each of the Bergen boxes controls one half of the chips. The two scintillators are connected to the Bergen boxes as well via the signal registration system. In this manner, the Bergen boxes can connect a trigger to the associated data.

The Bergen boxes are connected to the FoCal Data Acquisition system (FoCalDAQ) as well. This system contains software to access, process and analyse data and it is used to control measurements. A scheme of all the connections in the experimental setup is shown in Fig. 3.3.

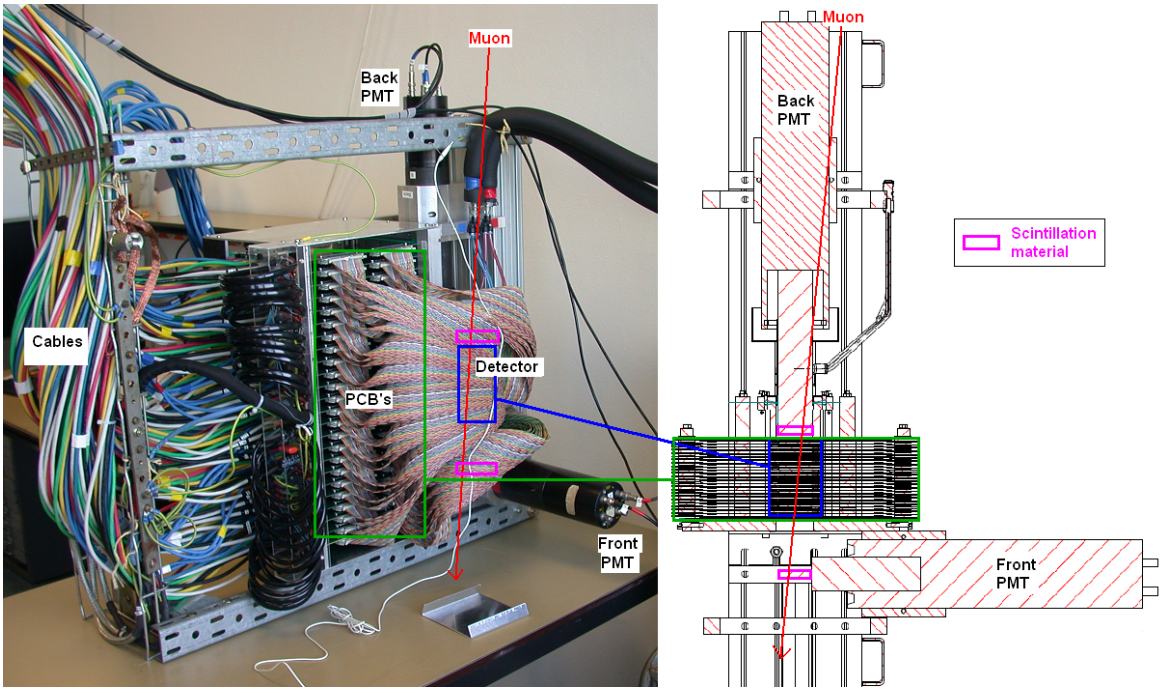

Figure 3.1: A picture (left) and a drawing (right) of the experimental setup. The FoCaL detector (blue box) is positioned behind the small cables in the picture and the Back and Front scintillator systems (magenta boxes) are above and below it. The red arrow represents a hypothetical trajectory of a cosmic muon. The green boxes mark the printed circuit boards that are connected to the chips. The layers of the detector are represented by the horizontal black lines in the blue box of the drawing.

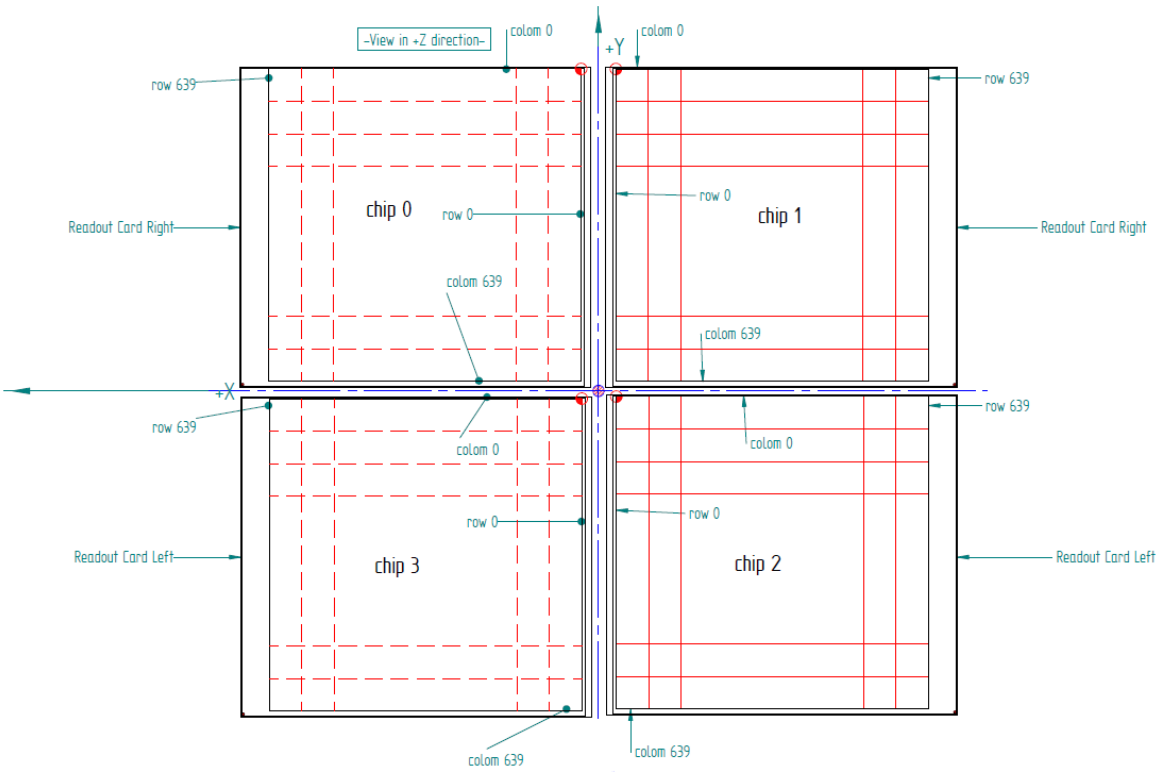

Figure 3.2: A schematic drawing of a layer of four chips as present in the FoCal prototype detector.

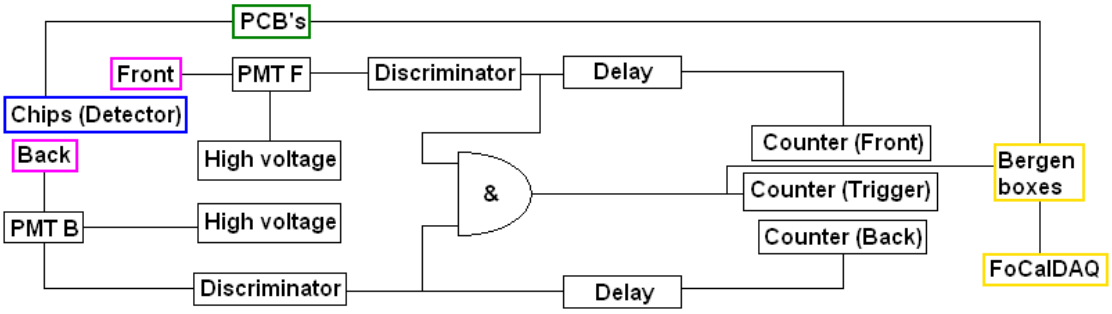

Figure 3.3: Connection scheme of all the parts present in the experimental setup. All the parts in black boxes are part of the signal registration system.

3.1.2 Chips

The FoCal prototype detector uses PHASE-II MIMOSA23 MAPS chips designed by the Institute Pluridisciplinaire Hubert Curien (IPHC) [6]. Chips with three different thicknesses of active silicon are used; with 14 μm, 15 μm and 20 μm silicon.

A chip is 19.52 mm by 20.93 mm in size with an active area of 19.2 mm by 19.2 mm containing 640 by 640 square pixels by a 30 μm pitch. They can be read out with a frequency of 160 MHz. A picture taken under a microscope of a small part of two chips is shown in Fig. 3.4. Here a pixel, a line and a column are marked with different colors. Discriminators at the end of each column cannot be seen in this picture because only a small fraction of the chips is photographed.

The read-out of the chips is done for one line at a time. A line selection circuit selects a line in the chip. Then the signals of all the pixels in that line are sent over the columns to the discriminators at the end of each column. This is schematically drawn in Fig. 3.5. By selecting all the lines one by one from the first line to the last, the complete chip is read-out. The full read-out of a chip is called a frame. The 640 discriminators at the end of each column are grouped into four channels. Via these four channels the data is sent to the printed circuit boards.

The sensitivity of the chips can be tuned with two variables, *P1* and *P2*. These can been viewed as knobs as shown in Fig. 3.5. By setting these variables to a certain value, bias voltages (*Vref1* and *Vref2*) on the discriminators are regulated which alters the sensitivity of the chips. The threshold of a chip is determined by *P1*. *P2* is responsible for the uniform response on the chip sensitivity along the row.

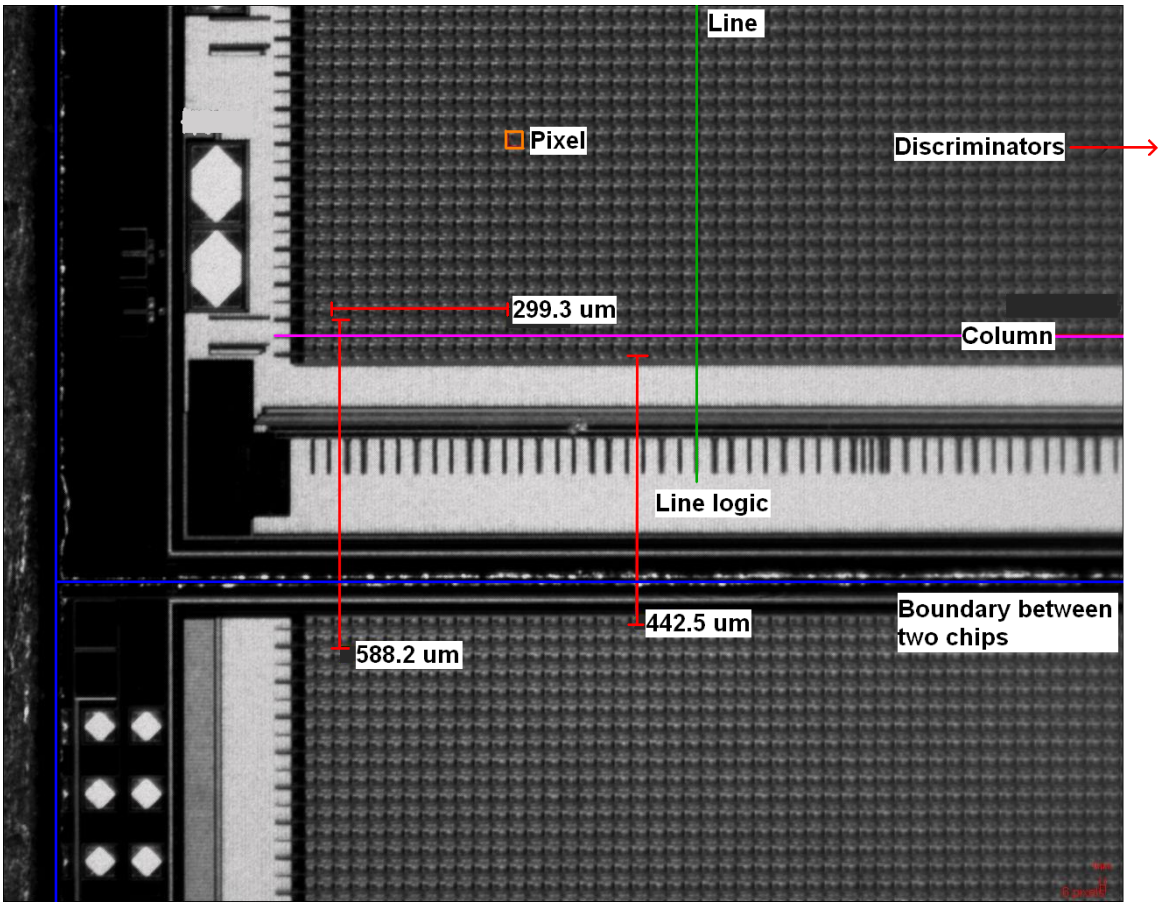

Figure 3.4: A picture of a part of two chips taken under a microscope. The lattice structure shows the pixels on the chips. One of pixels is marked with an orange box. The blue line represents boundary between the two chips. The red bars indicate some distances in μm. The green line marks a line of pixels and the magenta line marks a column of pixels on a chip.

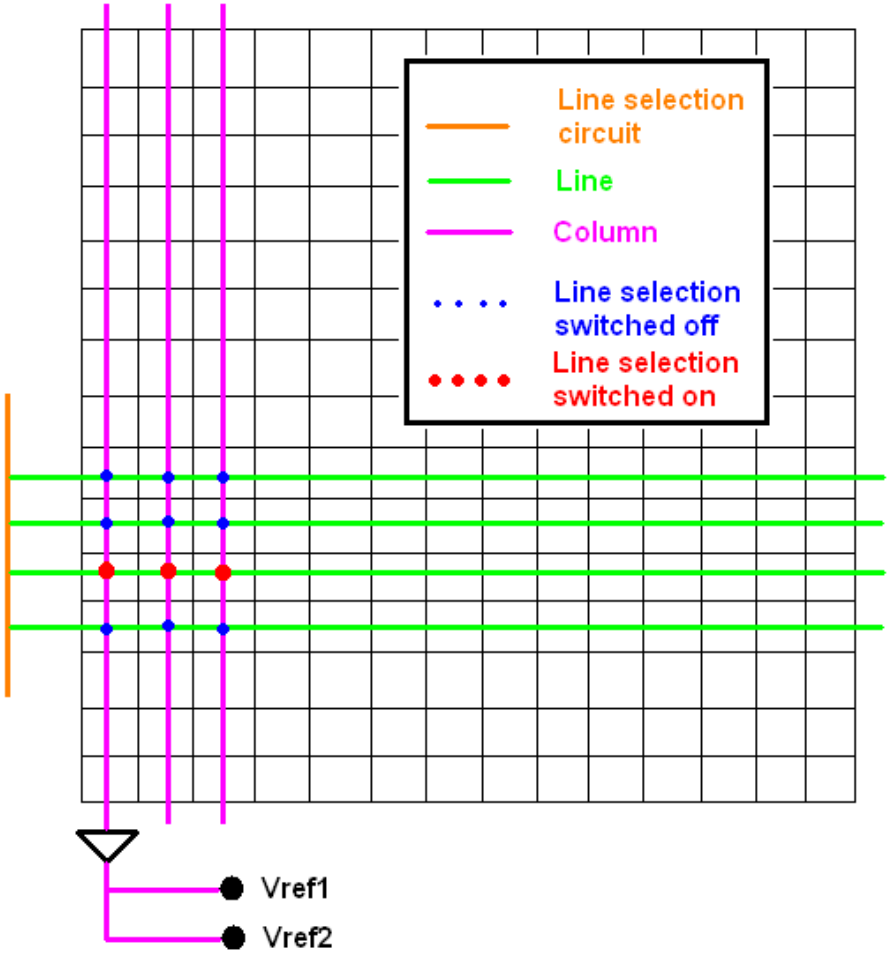

Figure 3.5: A schematic view of a MAPS chip as used in the FoCal prototype. Every square represents a pixel. The lines and columns are marked with the green and magenta lines respectively. Each line is connected to the line selection circuit which is orange in the drawing. The red and blue dots represent switches that can connect each column to a line in order to sent the signals of one line to the discriminators. In this picture there is one triangle at the end of one column representing one of the discriminators. The chip sensitivity (threshold) can be tuned by varying *P1* and *P2*. *P1* and *P2* are parameters for the bias voltages *Vref1* and *Vref2* which are represented by two knobs in the drawing.

3.2 Methods for measurements and analysis

3.2.1 Taking measurements

This section is divided in two subsections according to the different steps that have to be taken before and during the measurements. First the preferred settings are loaded on the chips. Then the measurement mode, pedestal or cosmics has to be chosen.

During the first research period a measurement was taken every day. Normally only *P1* was modified. In appendix A an overview of the taken measurements is provided and in appendix B the *P1* values used are listed.

Loading the chip settings

Before starting a measurement the chosen settings have to be loaded on the chips. This happens by editing a text file and loading it on the Bergen boxes. This procedure is only needed when new settings have to be loaded otherwise one can immediately continue with the selection of the type of measurement.

Choosing a measurement mode

Their are two measurement modes used during the studies described in this report. These are Cosmics mode and Pedestal mode:

- *Cosmics* All data are continuously written to the buffer of the Bergen boxes and the read-out of this buffer is trigger driven. Only data belonging to a trigger is shipped to the FoCalDAQ hard disk when the buffer is full.
- *Pedestal* All data are continuously written to the buffer and all data is shipped to the FoCalDAQ hard disk when the buffer is full.

Every measurement mode has a different purpose. When measuring cosmic radiation one only wants to collect data from particles. This data can be selected by the use of triggers and that is done in cosmics mode. During every cosmic radiation measurement the detector measures noise too. The noise has to be subtracted from the data because it is not part of signal of the particle. Therefore the noise has to be measured and that is done in pedestal measurement.

Since the Bergen boxes control the chips they are responsible for setting and maintaining a measurement mode. A complete measurement is called a run.

3.2.2 Analysing data

The data of the chips is sent to the Bergen boxes via the four channels of the chips (see Section 3.1.2). To make the data from the detector in a format that can be analysed it needs to be processed or, demultiplexed. Demultiplexing is a data formatting process. It has to be done for pedestal runs as well as for cosmic radiation runs.

The software that performs the analysis provides the data in files. In case of the pedestal runs these files contain the amount of noise per chip. When there is too much noise in a chip, a fraction of the noisy pixels is excluded. These excluded pixels will not be present in the cosmic radiation files. The process in which it is decided which pixels should be excluded can be explained as follows.

The data of the pedestal measurement is analysed by calculating the fraction of the time each pixel was active during the pedestal run. This results in a spectrum for each chip. A hypothetical example of such a spectrum is shown in Fig. 3.6. Then a weighted integration is performed over the spectrum from 0 to a certain value x'. When the weighted integral reaches a value $10^{-5} \cdot N_{pixels}$ (with N_{pixels} being the total number of pixels in a chip (640×640) and 10^{-5} being a restriction on the amount of noise) the integration stops. This point is called x'. The pixels on the right side of x' are excluded from further analysis (orange area).

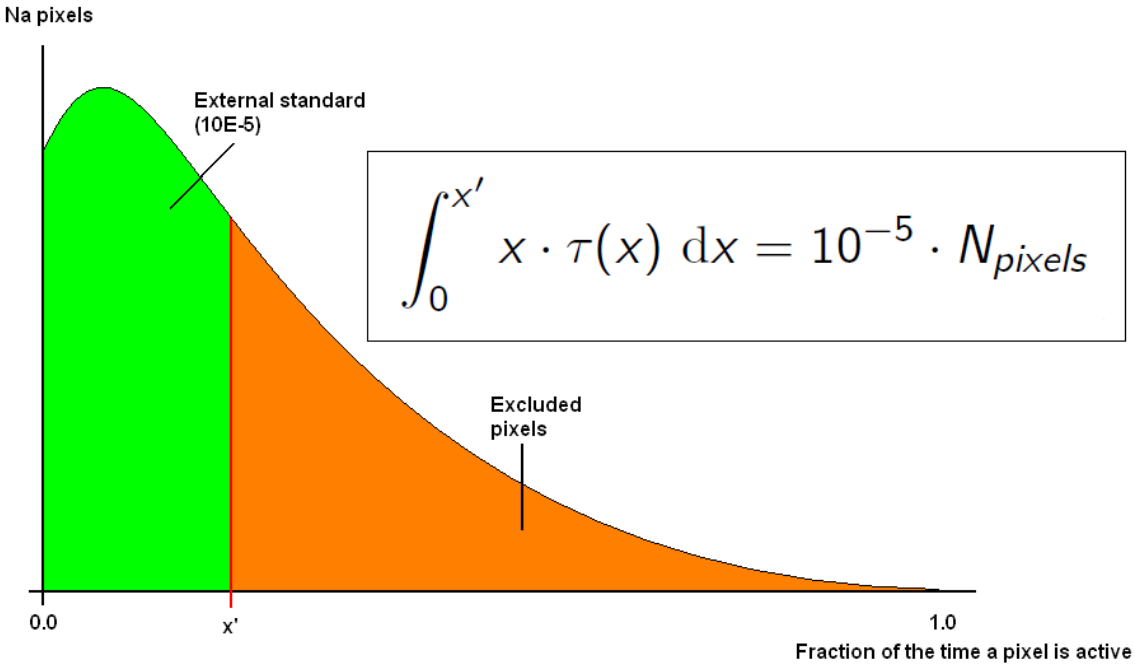

Figure 3.6: Hypothetical results of a hypothetical pedestal measurement for one chip. On the x-axis, the fraction of the time a pixel is active ($\tau(x)$) is shown and on the y-axis the number of pixels with a certain active time is presented (N_a). The integral in de box is the weighted integral performed by the pedestal software. Here N_{pix} is the total number of pixels on a chip (640×640).

In the analysis process the pedestal files are used to produce the cosmic radiation files. The excluded pixels (see Fig. 4.2) are not considered in the cosmic radiation analysis which leaves the cosmic radiation data with less noise.

The analysis continues by searching for tracks associated with trigger signals (each trigger refers to a coincidence of the scintillators signals that reveals the transit of a muon through the detector). The activation of one or few pixels in correspondence with a trigger signal indicates the transit of a muon. The tracker software searches for these pixels or hits. The search area on a chip is a circular area with a 1 mm radius. The location of this search area is affected by the location of the hits in the chips above and below it. The muon transits the detector in a straight line which means the hits on different chips should be on a straight line too and so does the search area.

Chapter 4

Detector performance

During the FoCal performance analysis three specific items were investigated; stability in time (measurement reproducibility), trigger losses and lost tracks. These items are reported in three sections. The first section is about the detector stability. In this section there is also a description of the quality of the chips since this influences the detector's stability. The last two sections are about the triggers losses and the lost tracks during measurements.

4.1 Detector stability

4.1.1 Goals

The goals of this measurement are to determine whether the detector is stable in time and to identity dead and bad chips. A chip is dead when it shows no activity and it is bad when it is unstable either in time or in output signal.

4.1.2 Methods

The detector is stable when it produces the same results for different measurements with the same settings. Therefore the stability of the FoCal prototype detector was determined by comparing pedestal runs with the same *P1* chip settings to see whether the results from these measurements were similar (see Appendix A and B). The comparison of the pedestal results was based on the median of the noise in each chip. This median noise was calculated in the following way.

During a pedestal measurement the fraction of the time a pixel is active in a chip can be calculated by dividing the number of frames a pixel was active in by the total number of frames collected in the measurement. This fraction is called the noise and it can be presented in a 2D-histogram. An example of such a histogram is given in Fig. 4.1(a); every point represents a pixels and the color of a point indicates the fraction of the time that the pixel was active during the pedestal measurement.

Then the noise is projected on the discriminator axis (there is a discriminator at the end of each column, therefore the term discriminator axis is used). This results in a histogram that shows the amount of noise per discriminator on a chip, as shown in Fig. 4.1(b).

From this projection histogram, a spectrum can be made. This spectrum contains the noise on the x-axis and the frequency on the y-axis. The frequency is the number of times a noise value is present in the projection histogram. An example spectrum is shown in Fig. 4.1(c). From this spectrum the median of the noise per chip can be calculated since the median is defined as the value that specifies the point between the lower and the higher half of a distribution.

The median of the noise per chip was compared for different pedestal runs with the same *P1* settings. This was done for all sets of settings (Appendix B). This resulted in a 3D-picture of the stability per chip for each set of settings. From this picture, bad and dead chips could be recognised. These chips either gave different results for measurements with equal settings, therefore the chips were not stable in time which makes then bad chips. Or they had zero median noise for all measurements which means they are inactive or, dead.

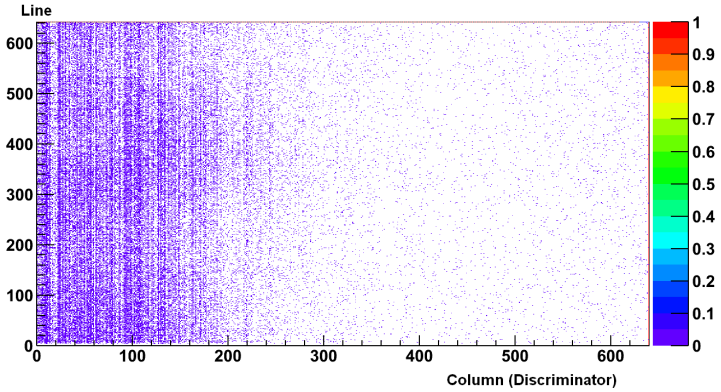

(a) Noise of one chip, calculated from a pedestal measurement. The colors indicate the fraction of the time a pixel was active during the measurement.

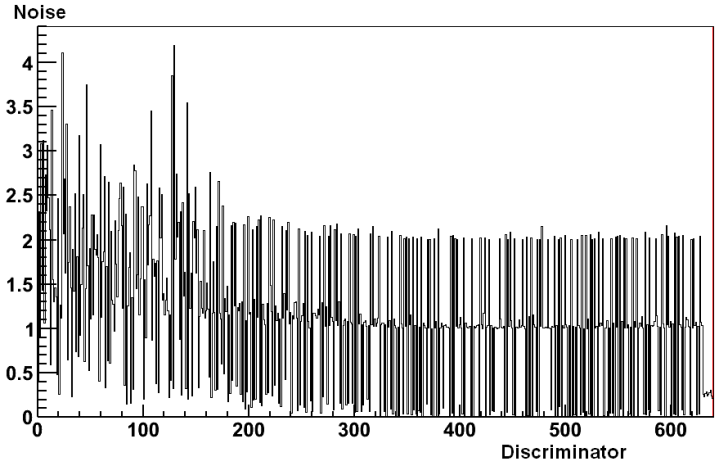

(b) Projection of the noise in a chip on the discriminator axis.

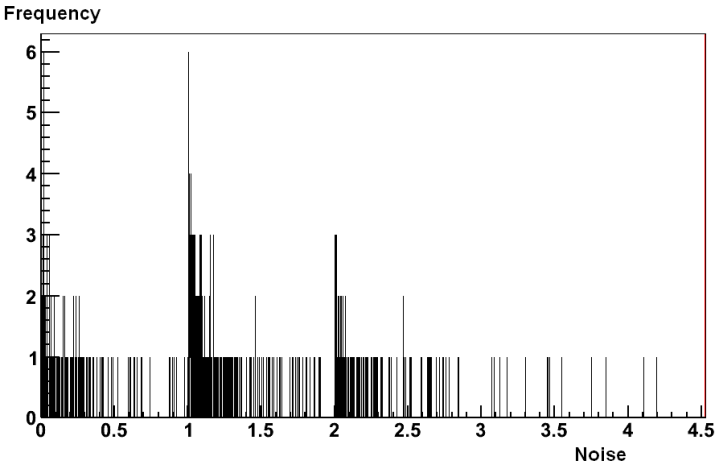

(c) Spectrum of the noise in a chip.

Figure 4.1: The three steps of calculating the median of the noise for a chip. Fig. 4.1(a) shows the noise in one chip. This noise is projected on the discriminator axis which results in the histogram of Fig. 4.1(b). With this projection a noise spectrum is made, see Fig. 4.1(c).

In order to come to a complete list of the dead and bad chips, the results of the pedestal measurements were compared to the results of the cosmic radiation measurements with the same settings. From these cosmics measurements the number of muon hits in a chip (M_h) was counted for each muon track. If a muon went through a chip, the number of hits detected in that chip was M_h. Then the number of times a certain value of M_h was found in that chip was counted and displayed into a histogram. If a chip is dead, the number of muon hits M_h is always zero. If it is bad, it has low M_h values in cosmics measurements.

4.1.3 Results

The median of the noise per chip for one set of chip settings is shown in Fig. 4.2. For most chips the median noise value is constant in time. Some chips have a median noise value that varies in time, for example chip 16 which is marked with the red arrow. Other chips, like chip 64 which is marked by the blue arrow, have no noise.

Fig. 4.3 shows the results of the cosmic radiation measurements for one set of chip settings. Here chip 16 and 64 are again marked with a red and blue arrow respectively. Chip 64 had zero muon hits every time a muon went through it as well as zero median noise which means it is dead. Chip 16 has reasonable muon hits numbers but it shows different median noise results for comparable pedestal measurements which means it is a bad chip.

All sets of chip settings were analysed and it was found that chips 25, 51, 64 and 76 never show any activity and therefore they are considered dead. Chips 16, 18, 20, 23, 40, 47, 59, 65, 72, 74, 90 and 94 have noise as well as muon hits but they are not stable in time (see Fig. 4.2) and therefore they are considered bad chips.

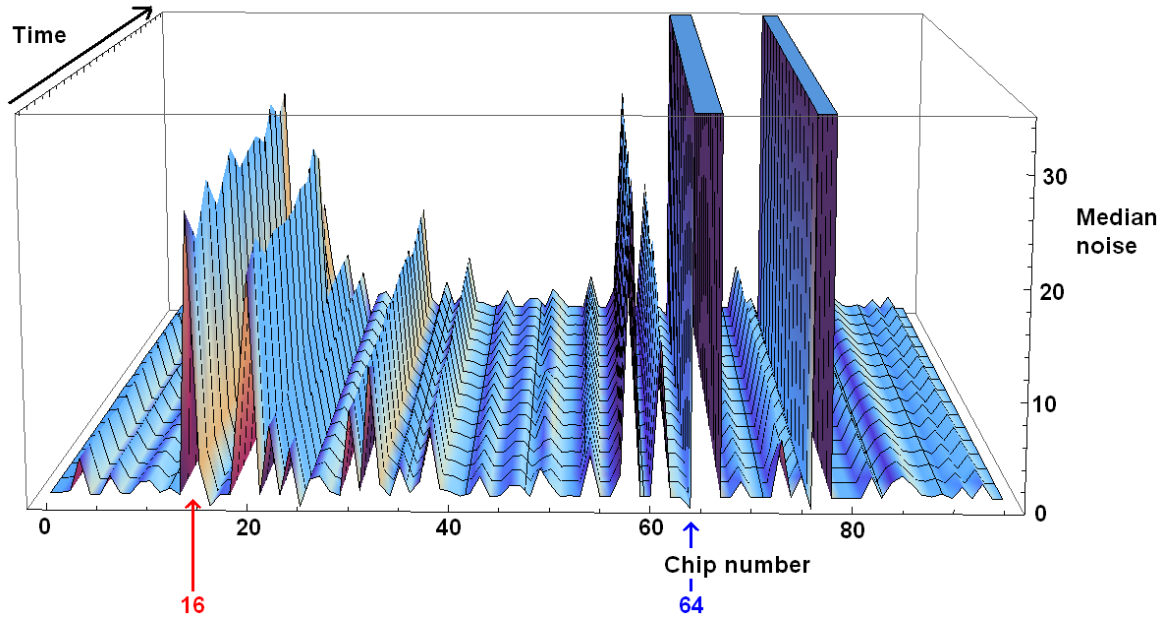

Figure 4.2: The median of the noise per chip in time for one set of chip settings. The arrows mark a dead chip (blue) and a bad chip (red).

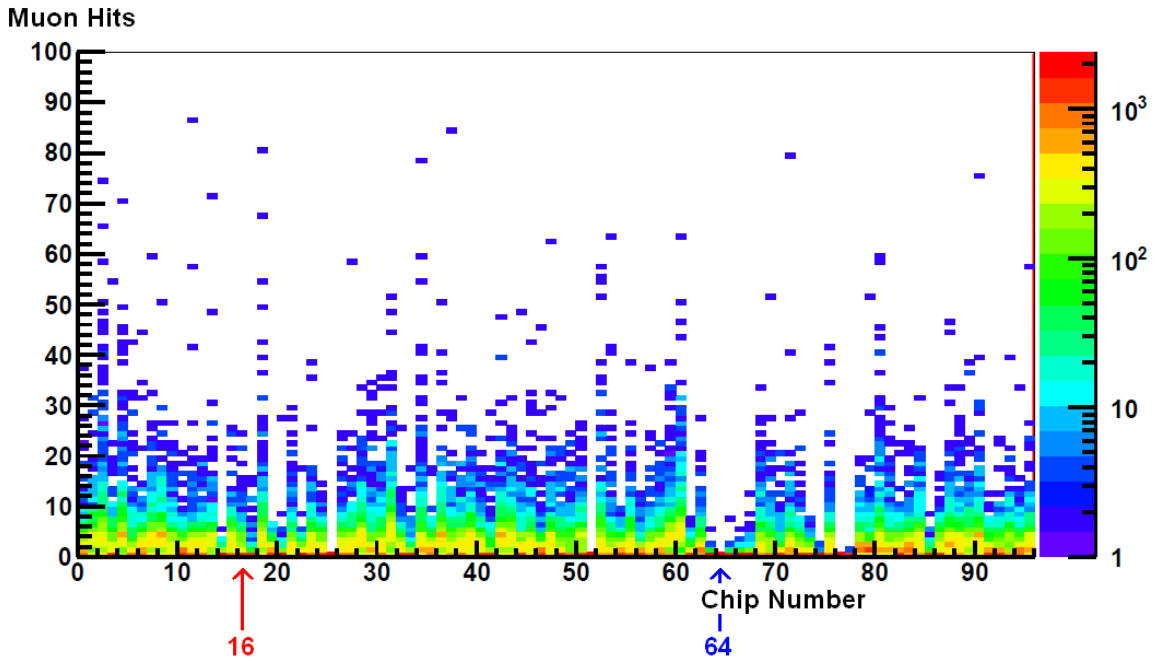

Figure 4.3: The number of muon hits per chip for one set of chip settings. The color indicates the number of times a muon hits value (M_h) was present in the chip. Again the blue arrow marks a dead chip and the red arrow a bad chip.

4.1.4 Discussion and conclusion

Finding a measure for the noise in a chip is difficult and the median of the noise may not be the best way to represent it. On the other hand, calculating the average from the noise spectrum (see Fig. 4.1(c)) as a measure for the noise in a chip is misleading in a lot of cases. Sometimes one area of a chip is damaged or one of the channels is broken and this affects the active time of those damaged pixels. This results in extreme values of the average of the noise. When using the median of the noise this effect is less and that is why it is used in this study.

Chips that produce different results in time are called bad chips and chips that produce no results are called dead chips. The dead chips are chips 25, 51, 64 and 76 and the bad chips are 16, 18, 20, 23, 40, 47, 59, 65, 72, 74, 90 and 94. An important result of this investigation is that, apart from the dead and bad chips, the detector is stable in time.

4.2 Lost triggers

4.2.1 Goals

The goals of this measurement are to determine the number of triggers and the signal frequencies of Front and Back. Then it will be determined for how many triggers data was written to the hard disk of FoCalDAQ. Comparing the trigger frequency with the frequency of triggers being recorded on FoCalDAQ gives the percentage of triggers that are lost during a measurement which is another goal of this measurement.

4.2.2 Methods

First the frequencies of the signals of Back and Front and the frequency of triggers were measured. This was done with the signal registration system that registers the number of Back and Front signals as well as the number of triggers over a time period (Section 3.1.1). A trigger is the coincidence in

time of the Back and Front signals which is caused by a muon transiting through the FoCal prototype. The pulse-registration system was repeatedly set to count the pulses of Back and Front for 2.5 h, which lead to a total measuring time of 710 h (612000 s).

The frequency measurements were always performed during a cosmics measurement. This allows for a comparison between the number of triggers and the number of recorded triggers. When a trigger occurs, the corresponding data is recorded with a time stamp. With this information it was possible to determine the number of triggers recorded during the frequency measurements.

4.2.3 Results

Table 4.1 summarizes the results from the frequency measurements. The frequency of Front is almost twice the frequency of Back. Furthermore there is a discrepancy between the trigger frequency and the recorded trigger frequency.

Table 4.1: Results of the frequency measurements of Back, Front, the triggers and the recorded triggers.

System	**Counts (#)**	**Frequency (Hz)**
Back	$(7.133 \pm 0.008) \cdot 10^5$	1.166 ± 0.001
Front	$(1.2746 \pm 0.0011) \cdot 10^6$	2.083 ± 0.002
Triggers	$(5.70 \pm 0.08) \cdot 10^3$	$(9.3 \pm 0.1) \cdot 10^{-3}$
Registered triggers	$(5.46 \pm 0.07) \cdot 10^3$	$(8.9 \pm 0.1) \cdot 10^{-3}$

4.2.4 Discussion and conclusion

Frequency measurement

As it can be seen from Table 4.1, Front has a pulse frequency twice as high as Back. For Front this frequency is 2.083 ± 0.002 Hz and for Back it is 1.166 ± 0.001 Hz. The frequency of the triggers ($f_t = (9.3 \pm 0.1) \cdot 10^{-3}$ Hz) is much lower than the frequencies of the scintillators output signals. A possible explanation for this could be the fact that the signals from the scintillators have a noise component due to a possible light leakage or high dark current.

Trigger efficiency

During cosmics measurements $(5.46 \pm 0.07) \cdot 10^3$ triggers were recorded while there were actually $(5.69 \pm 0.08) \cdot 10^3$ triggers. One of the reasons for this difference is the dead time of the detector due to writing data on the hard disk and the resetting of the acquisition system. These processes take about 1 second. To make an accurate comparison between the trigger frequency and the recorded trigger frequency, the data need to be corrected for this dead time.

Since there were $(5.46 \pm 0.07) \cdot 10^3$ triggers written to the hard disk, the actual time that the acquisition system could record the triggers was $612000 - 5460 = 606540$ s. Therefore the real trigger recording frequency is $(9.0 \pm 0.1) \cdot 10^{-3}$ Hz. There is still a small discrepancy with the trigger frequency. From this difference the percentage of lost triggers can be calculated. The result of this is that 3 ± 2 % of the triggers is lost during cosmic radiation measurements. This loss could be caused by a synchronisation problem within the acquisition system and the digital read-out electronics but there could also be other problems. At the moment there is no clear explanation of what is causing the loss of triggers.

4.3 Lost tracks

4.3.1 Goals

In some cases there is data from a trigger where the FoCal tracker software is not able to reconstruct a track from. This is called a lost track and it is the goal of this measurement to determine the percentage of lost tracks in cosmic radiation measurements. When this percentage is known the next step will be to determine the track loss cause. With this purpose in mind, the amount of lost tracks due to detector geometry and to the accidental triggers will be calculated.

4.3.2 Methods

The percentage of lost tracks was determined by counting the number of triggers from which the FoCal tracker software was not able to reconstruct a track. This was done for the triggers in runs 83 to 95 for two different versions of tracker software (version code21022013 and version code13052013). In the pedestal runs, the tracker software does not find tracks as is expected.

Then the number of lost tracks caused by the detector's geometry was determined via a Monte-Carlo simulation. In this simulation there are two plates representing Front and Back and a three-dimensional block representing the detector. Front and Back both have a 40 mm by 40 mm surface and the detector has a 38.9 by 38.3 mm active surface and a depth of 116 mm. Back is placed 10 mm above the detector and Front is placed 70 mm below the detector. This is shown in Fig. 4.4.

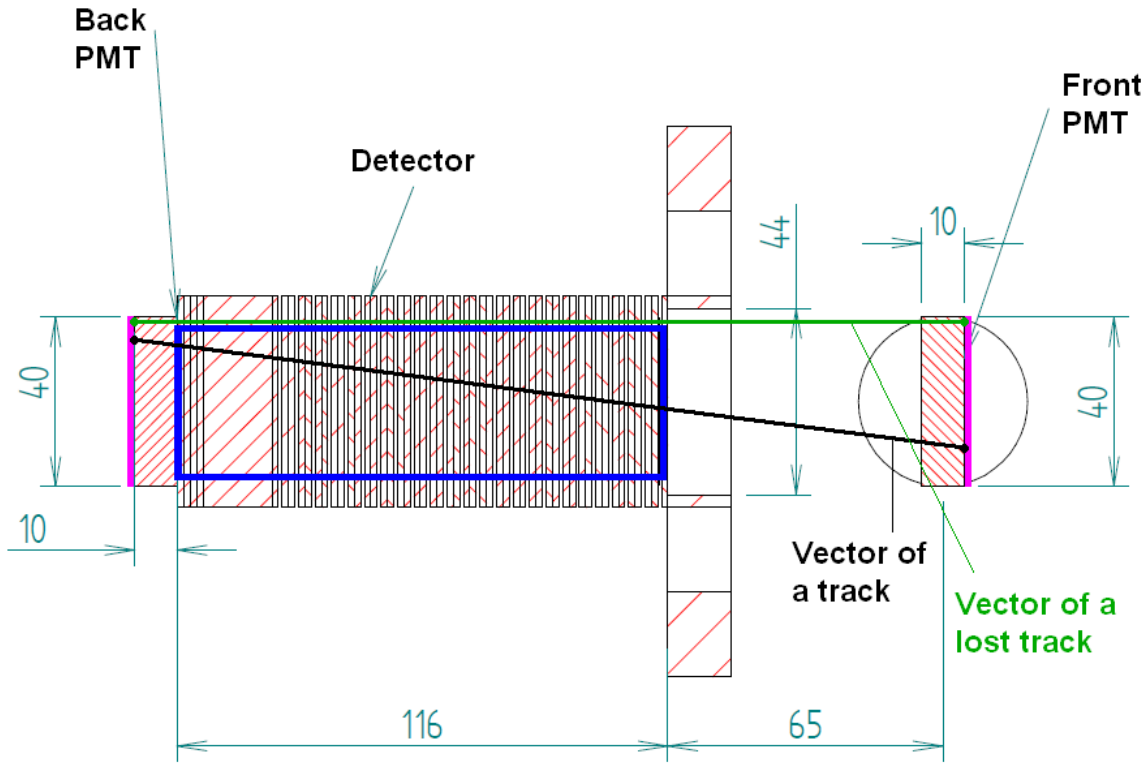

Figure 4.4: The detector's geometry. The Blue block represents the detector and the purple lines the two scintillator systems. The black and green line represent two vectors generated in the Monte-Carlo simulation. The green line represents a lost track which is caused by the geometry of the detector. The black line is a track which should not be lost because the detector's geometry.

During the simulation vectors are randomly generated in Front. When a vector ends at Back the simulation program calculates whether the vector went through the detector or not. The program counts the number vectors that ended at Back and went through the detector. The percentage of lost tracks caused by the detector's geometry is then given by

$$L_g = (1 - \frac{v_D}{v_B}) \cdot 100\% \tag{4.1}$$

where L_g is the percentage of lost tracks caused by detector geometry, v_D is the number vectors ending on Back and going through the detector and v_B the the total number of vectors ending on Back. The simulation was performed 15 times and each time 1020100 vectors ended on Back.

Accidental triggers cause lost tracks too. An accidental trigger is a trigger that comes from two noise signals instead of a muon. The probability for these accidental triggers is given by

$$P(\text{"accidental trigger"}) = f_F \cdot f_B \cdot \sigma \tag{4.2}$$

where f_F and f_B are the signal frequencies of Front and Back respectively and σ is the signal width of a signal of Front or Back. The signal frequencies are taken from the lost trigger measurement (see Table 4.1). The signal width of Front was measured with an oscilloscope.

4.3.3 Results

In Table 4.2 the percentage of lost tracks is shown. In this table it can be seen that for software version code21022013, (29 ± 2) % of the tracks is lost and that for software version code13052013 this percentage is (50 ± 3) %.

The results of the Monte-Carlo simulation are shown in Table 4.3. On average (1.012 ± 0.009) % of the tracks is lost because of the geometry of the detector.

The signal frequencies of Front and Back were measured in the trigger loss measurement (Table 4.1). The results of this measurement were $f_F = 2.083 \pm 0.002$ Hz and $f_B = 1.166 \pm 0.001$ Hz. The signal width was measured to be $(80 \pm 5) \cdot 10^{-9}$ s. Therefore the probability for an accidental trigger was $(1.942 \pm 0.003) \cdot 10^{-7}$ Hz (see Eq. 4.2) which is negligible compared to the trigger rate of 10−2 Hz.

4.3.4 Discussion and conclusion

There is a large difference in the percentage of lost tracks for the two different software versions. For software version code21022013, (29 ± 2) % of the tracks was lost and for software version code13052013 that was (50 ± 3) %. This is because of the changes made in the tracker software. The software searches for tracks in trigger data (see Section 3.2.2). For a track to be accepted by the software there have to be muon hits in different layers of the detector. In version code21022013 a track has to have at least 12 muon hits to be accepted. In version code13052013 a track has to have 24 muon hits in at least 12 different layers in order to be accepted. These different requirements in the different software versions cause the difference in the percentage of lost tracks.

Both the detector geometry and the accidental triggers cause only a small amount of lost tracks. The detector geometry causes (1.012 ± 0.009) % of the tracks to be lost and the probability for an accidental trigger is $(1.942 \pm 0.003) \cdot 10^{-7}$ Hz. As a result these two can not be causing the large percentage of lost tracks found in this measurement. As shown by the difference in lost tracks percentages of the two software versions, the software plays a major part in the amount of tracks that are found. In order to get a feeling of how big the contribution of the software to the lost tracks is, it might me helpful to look at pictures of tracks and see if tracks can be found by hand. This has not been done during this study.

Table 4.2: Percentage of lost tracks for runs 83 to 95.

		Software version code21022013		**Software version code13052013**	
Run	Number of Triggers	Number of Lost Tracks	Percentage of Lost Tracks	Number of Lost Tracks	Percentage of Lost Tracks
#	#	#	%	#	%
83	508	134	26.4	234	46,1
85	754	241	32.0	392	52,0
87	667	192	28.8	337	50,1
89	2105	610	29.0	1024	48,6
91	707	212	30.0	355	50,2
93	710	192	27.0	353	49,7
95	728	238	32.7	388	53,3

Table 4.3: Simulation results of the missing tracks due to detector geometry. Each time the simulation was performed, 1020100 vectors ended on Back.

Run	**Number of vectors missing the detector**	**Percentage of vectors missing the detector**
#	#	%
1	10291	1.0088
2	10341	1.0137
3	10358	1.0154
4	10361	1.0157
5	10374	1.0170
6	10216	1.0015
7	10389	1.0179
8	10389	1.0184
9	10370	1.0166
10	10181	0.9980
11	10502	1.0295
12	10309	1.0106
13	10279	1.0076
14	10180	0.9974
15	10362	1.0158

Chapter 5

Chip settings

To improve the performance of the FoCal detector prototype, the optimal chip settings have to be found. The chip settings are however not well understood which is a motivation to investigate them.

The chip settings can be set with the variables *P1* and *P2* (see Section 3.1.2). With these variable the threshold of a chip can be set which is given by *P1*. Furthermore *P2* is responsible for the uniform response on the chip sensitivity along the row. During the investigation described in this part of the report the properties of *P1* were investigated.

5.1 Goal

The goal of this measurement is to understand how varying *P1* affects the chip sensitivity. This is done by comparing the median of the noise, the number of excluded pixels and the cluster size of muon hits from different pedestal and cosmic radiation measurements.

5.2 Methods

Pedestal and cosmic radiation measurements were taken for eight different sets of chip settings (See Appendix A and B).

The original settings are Settings 1 which were determined before during previous investigations. The other sets of settings are variations on Settings 1 except for Settings 8. These settings were chosen after the analysis of Settings 1 to 7 based on the fact that these were the settings for which the chips performed best.

The analysis of all the measurements was done by determining the median noise value (Section 4.1.2), the amount of excluded pixels (Section 3.2.2) and the cluster size. The cluster size was calculated in the following way.

A cluster is a group of hits in one layer of the detector, belonging to one muon. The tracker software selects clusters according to certain criteria. Not only must the hits in a cluster be in the same layer, they have to be in a circle with a radius of 1 mm as well (Section 3.2.2). Another important criteria is that the hits in a cluster must be adjacent to each other. When the software has found clusters, the average cluster size of a chip is calculated which is the average number of hits in the cluster.

Sometimes when a muon traverses a chip, the software is not able to find hits in it. These zero's are left out in the calculation of the average cluster size. However these zero's are used to determine the percentage of zero muon hits when a track went through the chip, which is a measure for the chip's efficiency. The lower the percentage of zero muon hits, the more efficient a chip is. For all the different settings, the percentage of zero muon hits was calculated as well. In order to understand all the results better, pictures of the hit patterns of the chips were made as well.

5.3 Results

The results of the chip settings measurements are reported in three subsections. The first subsection is about the hit patterns of the chips resulting from pedestal and cosmic radiation measurements. The second subsection is about the results of the median noise, the excluded pixels and the cluster size calculations. The last section is about the percentage of zero muon hits in the chips.

5.3.1 The pedestal and cosmic radiation measurements

The hit patterns from one pedestal measurement (run 119) and those from cosmic radiation measurements 119 to 155 are shown in Fig. 5.1 and 5.2.

There are a few features in the hit patterns that stand out. The first is that every chip looks different in both the pedestal and the cosmic radiation measurements. Some chips have noise evenly spread over their whole surface while in other chips a gradient in the noise is seen, like in chip 38. In de pedestal measurement, some chips have red lines or columns which means that this line or column is active a hundred percent of the time. The gradients and the red lines are not visible in the cosmic radiation measurements. This is partially because of the pixels that are excluded during the pedestal analysis (Section 3.2.2).

In both the pedestal and the cosmic radiation measurements there are inactive channels visible, these are marked with a green box in the figures. For chip 47, one channel is inactive during pedestal measurement 119 but it does however contain muon hits as is seen in Fig. 5.2. Chip 47 is one of the bad chips (see Section 4.1); part of the chip is not working all the time which makes it unstable in time.

At last, in the cosmic radiation measurements there is this effect that in one of the corners of a chip there are less hits. This can be explained by the position of the chips in a layer. In Fig. 5.3 the muon hits in one layer are displayed for the runs 119 to 155. Here the corners contain less muon hits as well. This can be explained by the shape of the detector as shown in Fig. 5.4. The black lines which represent hypothetical muon tracks mostly hit the detector in the middle causing less muon hits at the edges of the detector.

Analysing the hit patterns for all the chips reveals again that chips 25, 51, 64 and 76 are dead and that chips 16, 18, 20, 23, 40, 47, 59, 65, 72, 74, 90 and 94 are bad.

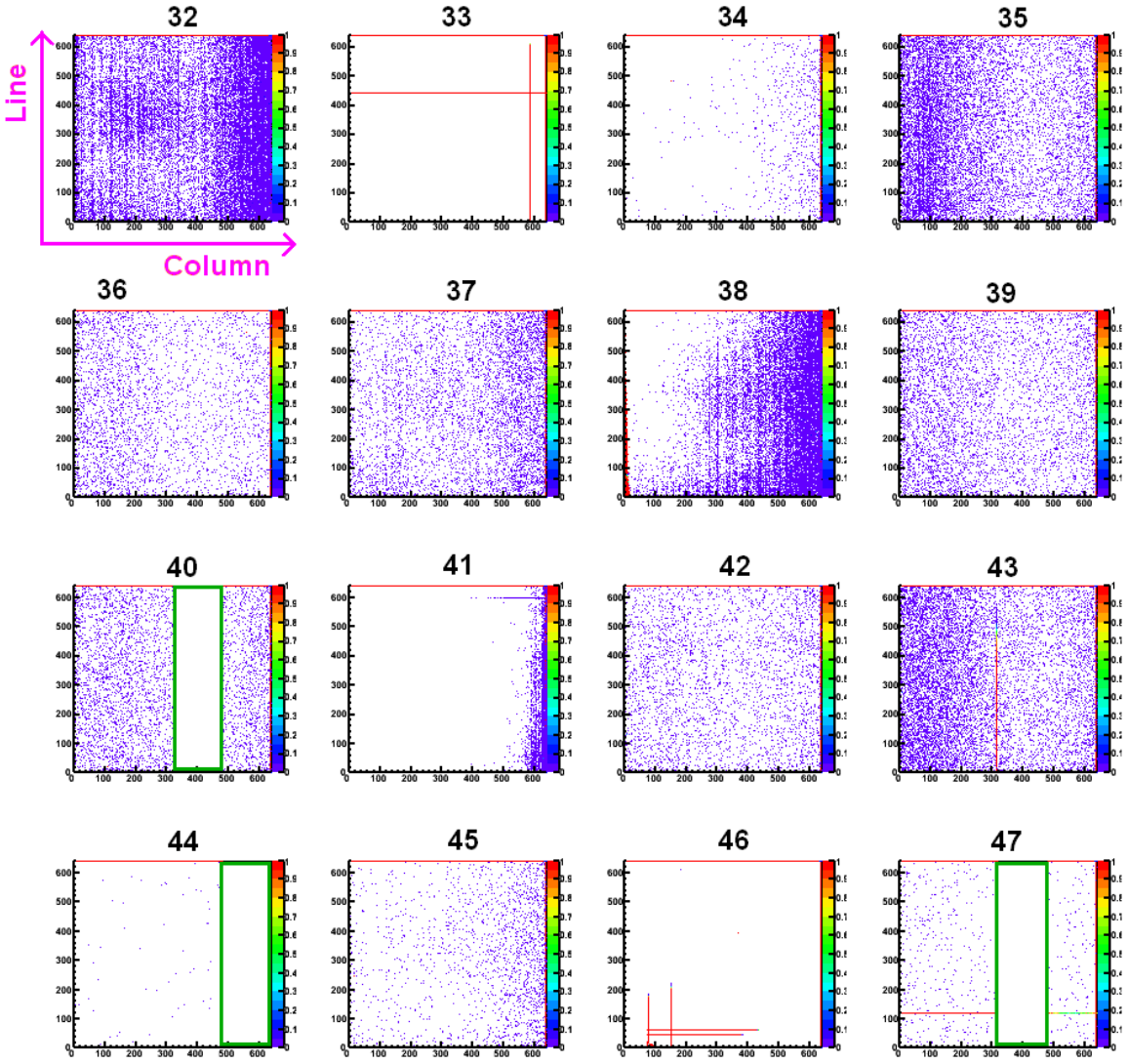

Figure 5.1: The noise hits of 16 chips for pedestal run 119. The colors indicate the fraction of the time a pixel was active during the run. The magenta axes next to the top left chip show the coordinates on the axes of every picture. An inactive channel is marked with a green box. Red lines in the pictures are lines or columns that are active a hundred percent the time.

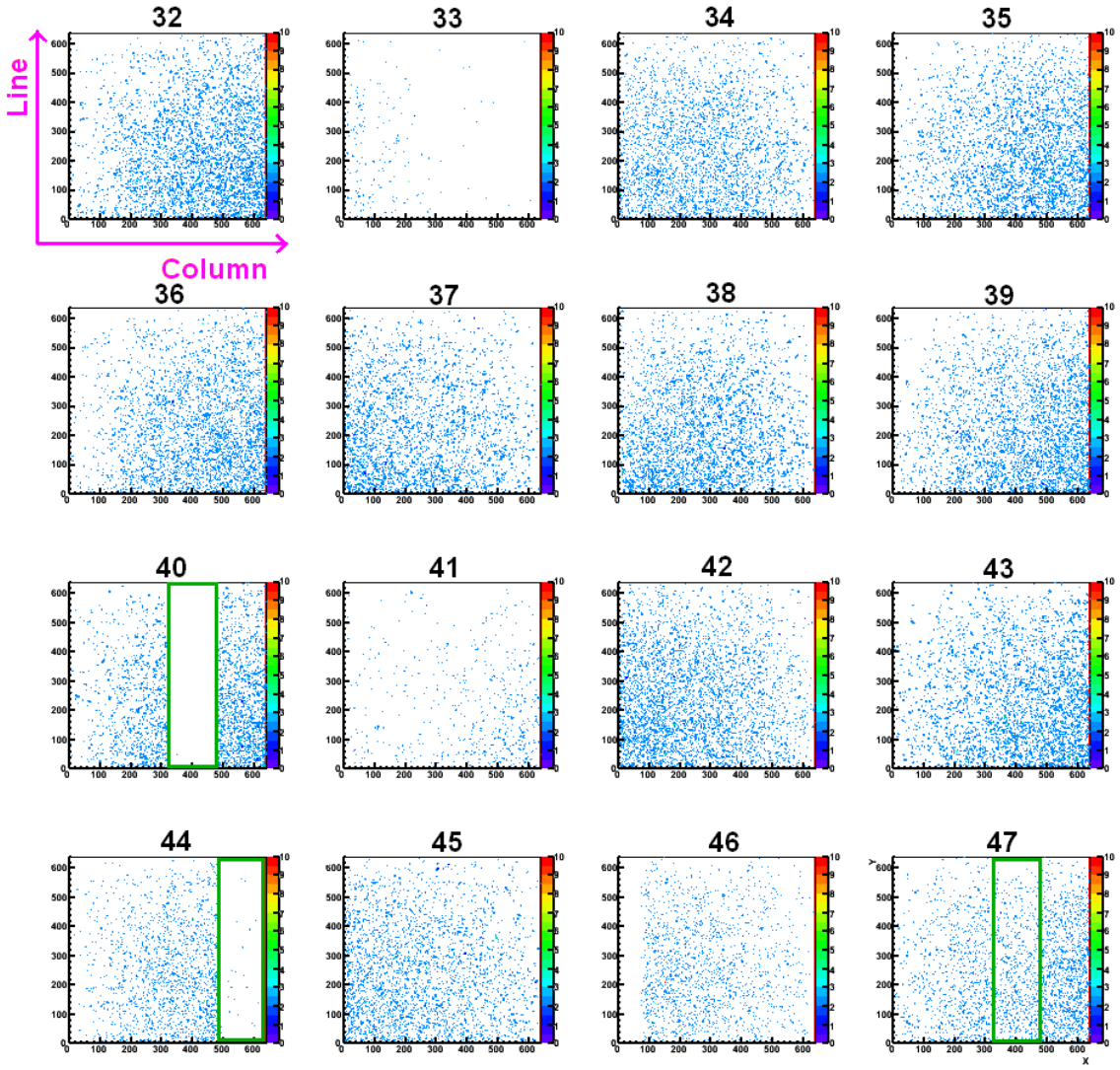

Figure 5.2: The muon hits for runs 119 to 156 (13,307 triggers). The colors indicate the number of times a pixel was hit by a muon. The magenta axes next to the top-left chip show the coordinates on the axes of ever picture. An inactive channel is marked with a green box.

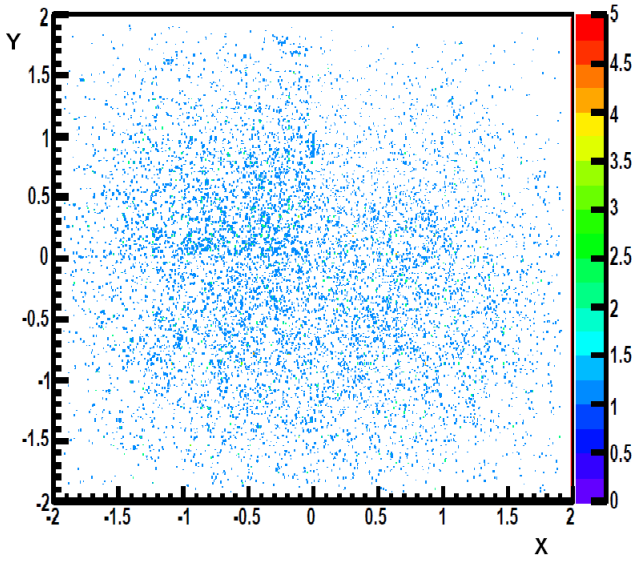

Figure 5.3: Muon hits in layer 3 for runs 119 to 156 (13,307 triggers). The color indicates the number of times a pixels is hit by a muon.

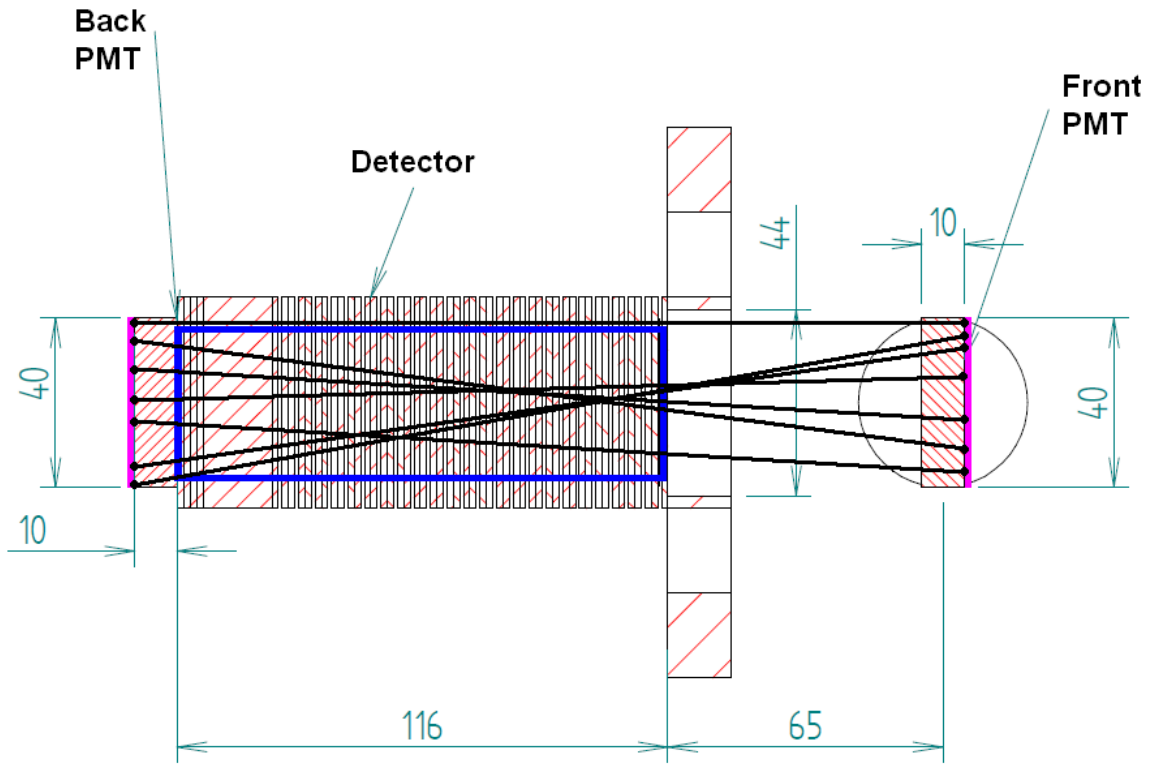

Figure 5.4: The shape of the detector affecting the positions of the muon hits. The black lines represent hypothetical muon tracks. From these hypothetical tracks it can be seen that detector is mostly hit in the middle.

5.3.2 Noise, excluded pixels and cluster size for different chip settings

In Fig. 5.5 the results of the median of the noise, the excluded pixels and the average cluster size calculations are shown for 16 chips. An overall effect caused by raising *P1* is that the median of the noise and the number excluded pixels both decrease. However this effect is visible in different parts of the *P1* regime for different chips. The cluster size varies more randomly with *P1*. For some chips, like chip 60, 71 and 84, the cluster size goes down when *Vref1* goes up but this is not a common feature of all chips. Furthermore the average cluster size never goes below 2 and it never exceeds 6.

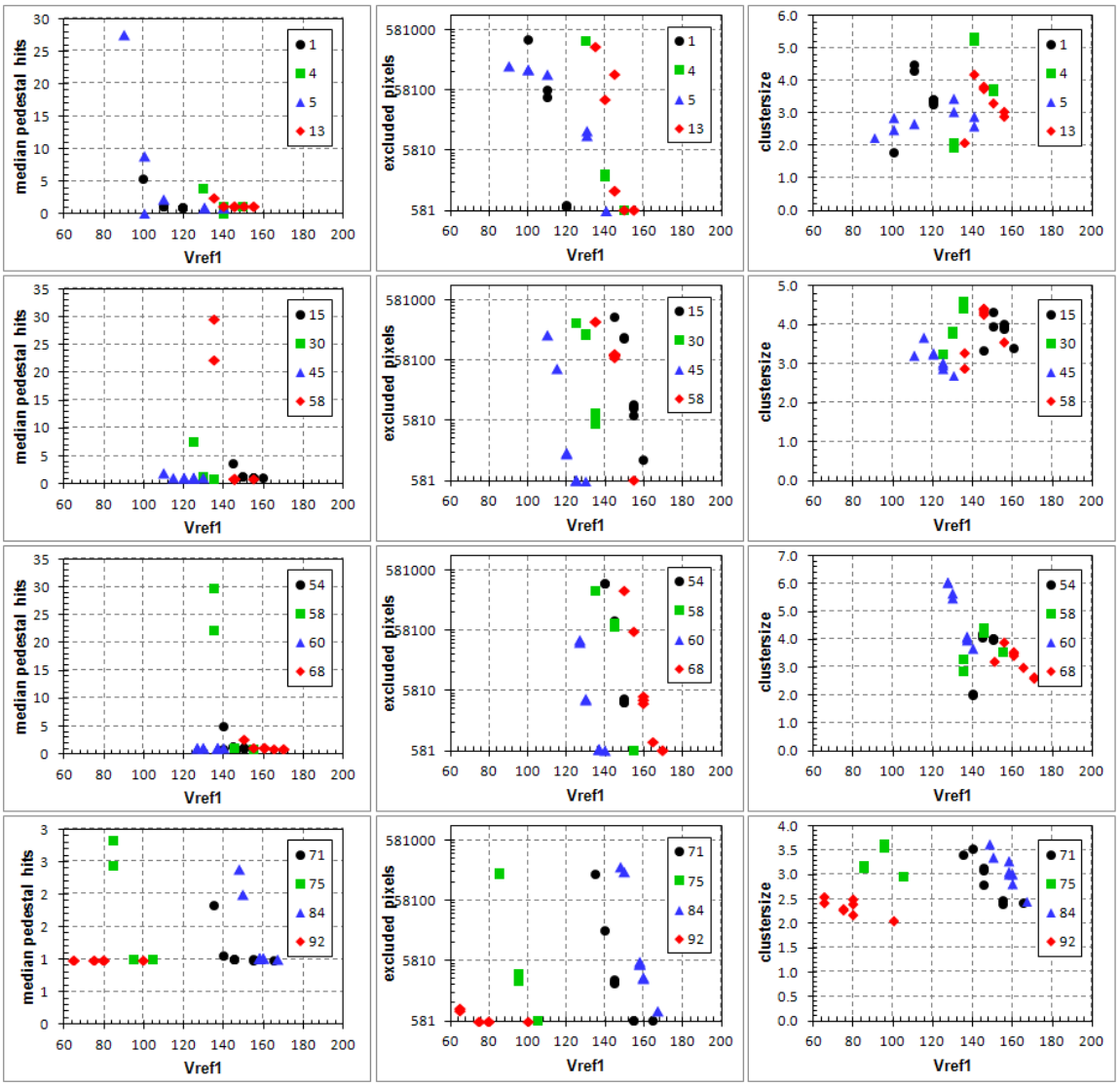

Figure 5.5: *P1* results for sixteen chips. From left to right: the median of the noise, number of excluded pixels and cluster size.

5.3.3 Chip efficiency

In Fig. 5.6 and 5.7 the percentages of zero muon hits when a track went through a chip, are shown for each chip and for each set of settings. The percentage of zero muon hits never goes below 10 %. Most chips have a percentage of zero muon hits for tracks in the region between 30% and 50%.

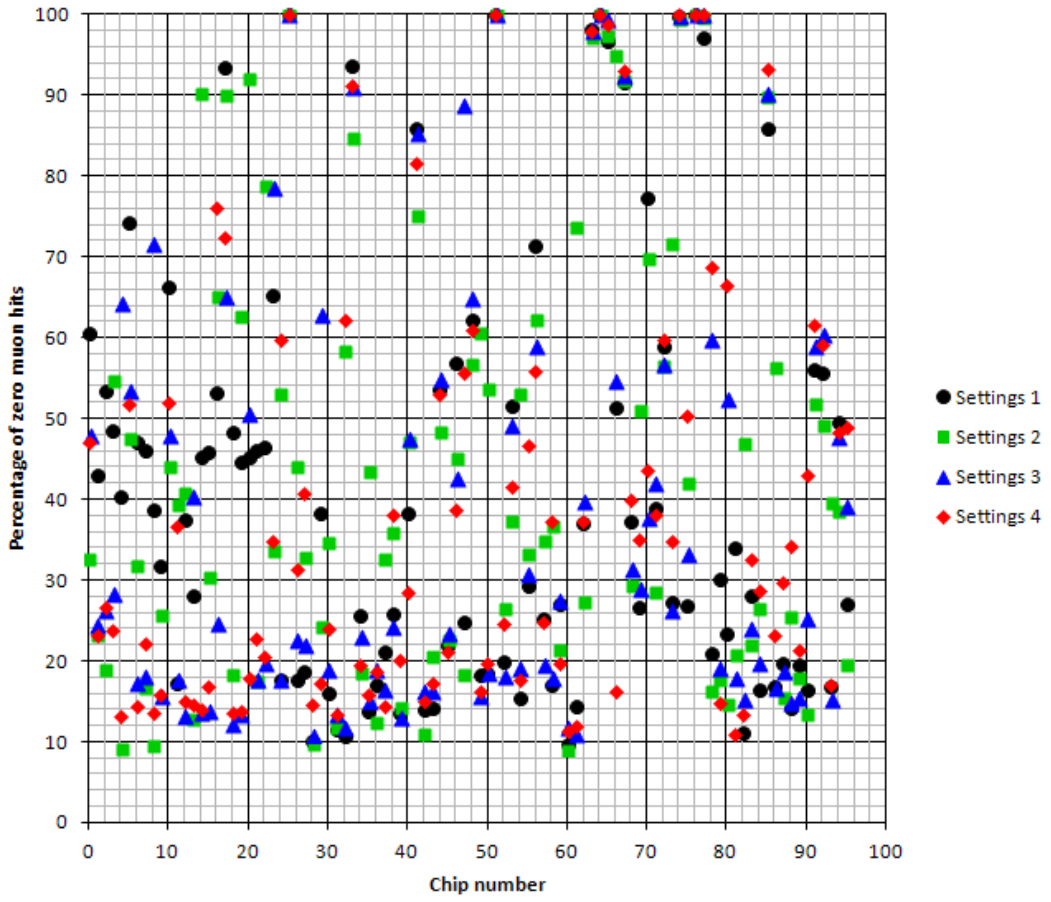

Figure 5.6: The percentage of zero muon hits for tracks, per chip, for settings 1, 2, 3 and 4.

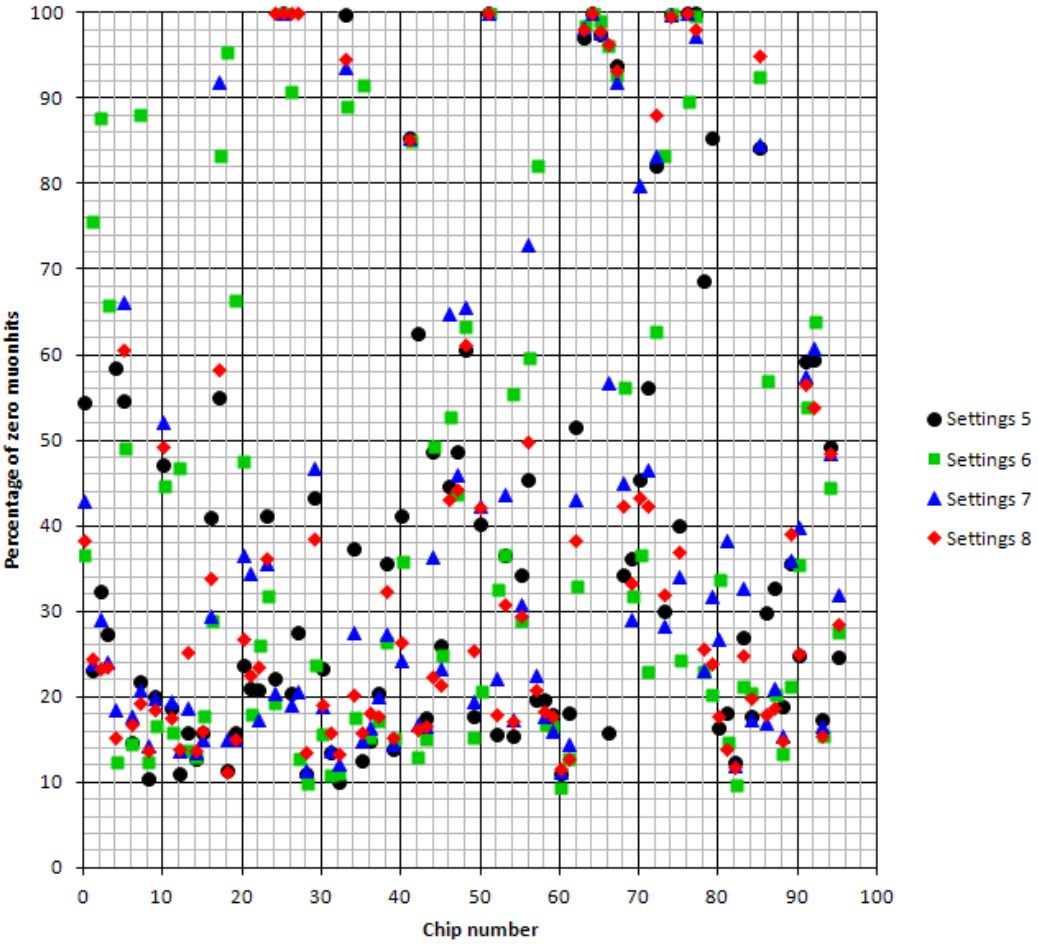

Figure 5.7: The percentage of zero muon hits for tracks, per chip, for settings 4, 5, 6 and 8.

5.4 Discussion and conclusion

The results of measurements for both pedestal and cosmic radiation measurements, differ from chip to chip. This is not only seen in the hit patterns of the chips but also in the median of the noise, the number of excluded pixels and cluster size calculations. Although different chips are sensitive around different *P1* values, patterns in how chips react to changes in *P1* have been found.

For most chips, when *P1* increases, the median noise and the number of excluded pixels both decrease. This does not hold for bad and dead chips. These chips respond very differently to changing the settings. For the cluster size there are no patterns found.

In both the cluster size and in the percentage of zero muon hits for tracks, a certain cut-off is found. For cluster size this cut-off is around 6 hits and for zero muon hits it is around 10 %. This means that chip efficiencies $(100 - H_z)$ above 90 % haven't been reached yet. For some chips, better *P1* settings have been obtained (see Fig. 5.6 and 5.7).

In the introduction *P1* was described as a sort of threshold value for the chips which can be confirmed after the analysis in this chapter.

Originally it was intended to change *P2* as well. Unfortunately, due to restrictions in the software which were revealed during the analysis of the measurements this has not been done during this investigation. For studies on the behaviour of the chips in relation with *P2* variation one can view the report of Roeland Nusselder.

Chapter 6

Conclusion

In this bachelor research the FoCal prototype detector performance and the tuning of the FoCal prototype detector with cosmic muons have been investigated.

It was found during the detector performance measurements that the stability in time of the detector is good except for the dead and bad chips. This is a very important result since the detector stability allows for the results to be reproduced. This is an essential feature for every measurement device for obvious reasons. Lost tracks remain a problem with the detector performance since it is not understood what causes the large amount them. Future research might contain a study on the triggers for which the software can not find tracks.

During the investigation of the chip settings there were patterns found in how *P1* is related to measurement results. When *P1* is increased, the median of the noise and the number of excluded pixels decrease. On the other hand, cluster size and detector efficiency both seem to be affected by a cut-off. Future research should determine whether these effects can be controlled or whether they could be related to the type of chips used in the prototype. From the results of the percentages of zero muon hits in a chip for tracks, it can also be seen that for some chips better settings have been obtained.

One of the problems with looking for patterns in chip sensitivity is that until now only a few chip settings have been tested and only *P1* has been investigated. One of the reasons for this is that cosmic muons enter the detector at a very low frequency (one muon in about two minutes). Another reason is that there has been a problem with the software that loads the settings on the chips. Therefore more research on tuning the FoCal prototype detector is necessary.

Bibliography

[1] Wikipedia. `http://en.wikipedia.org/wiki/File:Atmospheric_Collision.svg`. Accessed: 28-05-2013.

[2] The ALICE FoCal collaboration. Letter of Intent - A Forward Calorimeter (FoCal) for the ALICE experiment, February 2013.

[3] Particle Data Group. PDG july 2012 particle physics booklet. University of California, July 2012.

[4] Claus Grupen and Irene Buvat. *Handbook of Particle Detection and Imaging*. Springer-Verlag Berlin Heidelberg, 2012.

[5] Ernest M. Henly and Alejandro Garcia. *Subatomic Physics*. World Scientific, 2010.

[6] A. Himmi, G. Bertolone, A. Brogna, W. Dulinski, C. Colledaniand A. Dorokhov, Ch. Hu, F. Morel, and I.Valin. *PHASE-I User Manual Preliminary version*. IPHC, July 2008.

[7] Jean Letessier and Johann Rafelski. *Hadrons and Quark-Gluon Plasma*, chapter 1. Cambridge University Press, 2009.

[8] Donald H. Perkins. *Introduction tot High Energy Physics*, chapter 11. Cambridge University Press, 4 edition, 2012.

[9] R. Turchetta, J.D. Berst, B. Casadei, G. Claus, C. Colledani, W. Dulinski, Y. Hu, D. Husson, J.P. Le Normand, J.L. Riester, G. Deptuch, U. Goerlach, S. Higueret, and M. Winter. A monilithic active pixel sensor for charged particle tracking and imaging using standard VLSI CMOS technology. *Nuclear Instruments and Methods in Physics Research A*, 458:677–689, 2001.

Appendix A

Data overview

Table A.1: Data overview

Run	Mode	Start date	Stop date	Triggers	Details
83	Cosmics	05-02-2013	06-02-2013	510	
84	Pedestal	06-02-2013	06-02-2013	4	All chips were reset and configured.
85	Cosmics	06-02-2013	07-02-2013	755	
86	Pedestal	07-02-2013	07-02-2013	4	All chips were reset and configured.
87	Cosmics	07-02-2013	08-02-2013	667	
88	Pedestal	08-02-2013	08-02-2013	4	All chips were reset and configured.
89	Cosmics	08-02-2013	11-02-2013	2105	
90	Pedestal	11-02-2013	11-02-2013	4	All chips were reset and configured.
91	Cosmics	11-02-2013	12-02-2013	707	
92	Pedestal	12-02-2013	12-02-2013	5	All chips were reset and configured.
93	Cosmics	12-02-2013	13-02-2013	710	
94	Pedestal	13-02-2013	13-02-2013	6	All chips were reset and configured.
95	Cosmics	13-02-2013	14-02-2013	728	
96	Pedestal	14-02-2013	14-02-2013	4	All chips were reset and configured.
97	Cosmics	14-02-2013	14-02-2013	239	All chips are turned off.
98	Pedestal	15-02-2013	15-02-2013	4	All chips are configured.
99	Cosmics	15-02-2013	18-02-2013	2073	
100	Pedestal	18-02-2013	18-02-2013	4	All chips were reset and configured.
101	Cosmics	18-02-2013	19-02-2013	660	
102	Pedestal	19-02-2013	19-02-2013	6	All chips were reset and configured.
103	Cosmics	19-02-2013	20-02-2013	796	
104	Pedestal	20-02-2013	20-02-2013	—	An error occurred.
105	Pedestal	20-02-2013	20-02-2013	4	All chips were reset and configured.
106	Cosmics	20-02-2013	21-02-2013	818	
107	Pedestal	21-02-2013	21-02-2013	4	
108	Cosmics	21-02-2013	22-02-2013	—	An error occurred.
109	Pedestal	22-02-2013	22-02-2013	—	Wrong settings.
110	Pedestal	22-02-2013	22-02-2013	4	All chips were reset and configured.
111	Cosmics	22-02-2013	25-02-2013	2250	
112	Pedestal	25-02-2013	25-02-2013	—	Run failed.
113	Pedestal	25-02-2013	25-02-2013	—	Run failed.
114	Pedestal	25-02-2013	25-02-2013	49	To much triggers to be used properly.
115	Pedestal	25-02-2013	25-02-2013	4	
116	Cosmics	25-02-2013	26-02-2013	623	
117	Pedestal	26-02-2013	26-02-2013	4	

Table A.1: Data overview

Run	Mode	Start date	Stop date	Triggers	Details
118	Cosmics	26-02-2013	27-02-2013	666	
119	Pedestal	27-02-2013	27-02-2013	4	
120	Cosmics	27-02-2013	28-02-2013	661	
121	Pedestal	28-02-2013	28-02-2013	10	
122	Cosmics	28-02-2013	01-03-2013	683	
123	Pedestal	01-03-2013	01-03-2013	4	
124	Cosmics	01-03-2013	04-03-2013	355	A crash occurred during measurement.
125	Pedestal	04-03-2013	04-03-2013	4	
126	Cosmics	04-03-2013	05-03-2013	691	
127	Pedestal	05-03-2013	05-03-2013	4	
128	Cosmics	05-03-2013	06-03-2013	744	
129	Pedestal	06-03-2013	06-03-2013	4	
130	Cosmics	06-03-2013	07-03-2013	675	
131	Pedestal	07-03-2013	07-03-2013	4	
132	Cosmics	07-03-2013	08-03-2013	827	
133	Pedestal	08-03-2013	08-03-2013	4	
134	Cosmics	08-03-2013	11-03-2013	344	A crash occurred during measurement.
135	Pedestal	11-03-2013	11-03-2013	4	
136	Cosmics	11-03-2013	12-03-2013	738	
137	Pedestal	12-03-2013	12-03-2013	5	
138	Cosmics	12-03-2013	13-03-2013	833	
139	Pedestal	13-03-2013	13-03-2013	4	
140	Cosmics	13-03-2013	14-03-2013	789	
141	Pedestal	14-03-2013	14-03-2013	4	
142	Cosmics	14-03-2013	15-03-2013	670	
143	Pedestal	15-03-2013	15-03-2013	4	
144	Cosmics	15-03-2013	18-03-2013	2274	
145	Pedestal	18-03-2013	18-03-2013	4	
146	Cosmics	18-03-2013	19-03-2013	773	
147	Pedestal	19-03-2013	19-03-2013	4	
148	Cosmics	19-03-2013	21-03-2013	1338	
149	Pedestal	21-03-2013	21-03-2013	4	
150	Cosmics	21-03-2013	21-03-2013	—	Wrong settings.
151	Cosmics	21-03-2013	22-03-2013	725	
152	Pedestal	22-03-2013	22-03-2013	4	
153	Cosmics	22-03-2013	25-03-2013	712	A crash occurred during measurement.
154	Pedestal	25-03-2013	25-03-2013	6	
155	Cosmics	25-03-2013	25-03-2013	128	New chip settings loaded (Settings 2).
156	Pedestal	25-03-2013	25-03-2013	4	
157	Cosmics	25-03-2013	26-03-2013	736	
158	Pedestal	26-03-2013	26-03-2013	4	
159	Cosmics	26-03-2013	27-03-2013	840	
160	Pedestal	27-03-2013	27-03-2013	4	
161	Cosmics	27-03-2013	28-03-2013	676	
162	Pedestal	28-03-2013	28-03-2013	4	
163	Cosmics	28-03-2013	02-04-2013	3646	
164	Pedestal	02-04-2013	02-04-2013	—	Wrong settings.
165	Pedestal	02-04-2013	02-04-2013	4	
166	Cosmics	02-04-2013	03-04-2013	787	
167	Pedestal	03-04-2013	03-04-2013	4	

Table A.1: Data overview

Run	Mode	Start date	Stop date	Triggers	Details
168	Cosmics	03-04-2013	04-04-2013	761	
169	Pedestal	04-04-2013	04-04-2013	4	
170	Cosmics	04-04-2013	05-04-2013	735	
171	Pedestal	05-04-2013	05-04-2013	4	
172	Cosmics	05-04-2013	08-04-2013	1036	A crash occurred during measurement.
173	Pedestal	08-04-2013	08-04-2013	4	
174	Cosmics	08-04-2013	09-04-2013	844	
175	Pedestal	09-04-2013	09-04-2013	4	
176	Cosmics	09-04-2013	10-04-2013	754	
177	Pedestal	10-04-2013	10-04-2013	4	
178	Cosmics	10-04-2013	11-04-2013	803	
179	Pedestal	11-04-2013	11-04-2013	4	
180	Cosmics	11-04-2013	11-04-2013	111	New chip settings loaded (Settings 3).
181	Pedestal	11-04-2013	11-04-2013	2	Wrong settings.
182	Pedestal	11-04-2013	11-04-2013	5	
183	Cosmics	11-04-2013	12-04-2013	578	
184	Pedestal	12-04-2013	12-04-2013	6	
185	Cosmics	12-04-2013	15-04-2013	2265	
186	Pedestal	15-04-2013	15-04-2013	6	
187	Cosmics	15-04-2013	16-04-2013	237	Power outage.
188	Pedestal	16-04-2013	16-04-2013	4	
189	Cosmics	16-04-2013	17-04-2013	762	
190	Pedestal	17-04-2013	17-04-2013	4	
191	Cosmics	17-04-2013	22-04-2013	3721	
192	Pedestal	22-04-2013	22-04-2013	4	
193	Cosmics	22-04-2013	22-04-2013	99	Wrong settings.
194	Pedestal	22-04-2013	22-04-2013	4	New chip settings loaded (Settings 4).
195	Pedestal	22-04-2013	22-04-2013	4	
196	Cosmics	22-04-2013	23-04-2013	741	
197	Pedestal	23-04-2013	23-04-2013	6	
198	Cosmics	23-04-2013	24-04-2013	706	
199	Pedestal	24-04-2013	24-04-2013	4	
200	Cosmics	24-04-2013	25-04-2013	746	
201	Pedestal	25-04-2013	25-04-2013	4	All chips reset and configured.
202	Cosmics	25-04-2013	26-04-2013	696	
203	Pedestal	26-04-2013	26-04-2013	4	
204	Cosmics	26-04-2013	29-04-2013	2332	
205	Pedestal	29-04-2013	29-04-2013	4	
206	Cosmics	29-04-2013	01-05-2013	1617	
207	Pedestal	01-05-2013	01-05-2013	4	
208	Cosmics	01-05-2013	02-05-2013	733	
209	Pedestal	02-05-2013	02-05-2013	4	
210	Cosmics	02-05-2013	02-05-2013	711	
211	Pedestal	03-05-2013	03-05-2013	—	Wrong settings.
212	Pedestal	03-05-2013	03-05-2013	4	
213	Cosmics	03-05-2013	06-05-2013	2403	
214	Pedestal	06-05-2013	06-05-2013	4	New chip settings loaded (Settings 5).
215	Cosmics	06-05-2013	08-05-2013	1388	
216	Pedestal	08-05-2013	08-05-2013	4	
217	Cosmics	08-05-2013	13-05-2013	3690	

Table A.1: Data overview

Run	Mode	Start date	Stop date	Triggers	Details
218	Pedestal	13-05-2013	13-05-2013	4	
219	Cosmics	13-05-2013	14-05-2013	810	
220	Pedestal	14-05-2013	14-05-2013	5	
221	Cosmics	14-05-2013	15-05-2013	817	
222	Pedestal	15-05-2013	15-05-2013	4	
223	Cosmics	15-05-2013	16-05-2013	681	
224	Pedestal	16-05-2013	16-05-2013	4	New chip settings loaded (Settings 6).
225	Cosmics	16-05-2013	17-05-2013	736	
226	Pedestal	17-05-2013	17-05-2013	4	
227	Cosmics	17-05-2013	21-05-2013	3051	
228	Pedestal	21-05-2013	21-05-2013	4	
229	Cosmics	21-05-2013	22-05-2013	726	
230	Pedestal	22-05-2013	22-05-2013	4	
231	Cosmics	22-05-2013	23-05-2013	793	
232	Pedestal	23-05-2013	23-05-2013	4	
233	Cosmics	23-05-2013	24-05-2013	780	Power outage.
234	Pedestal	24-05-2013	24-05-2013	—	Wrong settings.
235	Pedestal	24-05-2013	24-05-2013	4	
236	Cosmics	24-05-2013	27-05-2013	2164	
237	Pedestal	27-05-2013	27-05-2013	4	
238	Cosmics	27-05-2013	28-05-2013	864	
239	Pedestal	28-05-2014	28-05-2013	4	
240	Cosmics	28-05-2013	29-05-2013	858	
241	Pedestal	29-05-2013	29-05-2013	4	
242	Cosmics	29-05-2013	30-05-2013	776	
243	Pedestal	30-05-2013	30-05-2013	4	
244	Cosmics	30-05-2013	31-05-2013	717	
245	Pedestal	31-05-2013	31-05-2013	-	New chip settings loaded (Settings 7).
246	Pedestal	31-05-2013	31-05-2013	4	
247	Cosmics	31-05-2013	03-06-2013	2156	
248	Pedestal	03-06-2013	03-06-2013	4	
249	Cosmics	03-06-2013	04-06-2013	811	
250	Pedestal	04-06-2013	04-06-2013	14	
251	Cosmics	04-06-2013	06-06-2013	1406	
252	Pedestal	06-06-2013	06-06-2013	4	
253	Cosmics	06-06-2013	07-06-2013	891	
254	Pedestal	07-06-2013	07-06-2013	5	
255	Cosmics	07-06-2013	10-06-2013	2206	
256	Pedestal	10-06-2013	10-06-2013	4	
257	Cosmics	10-06-2013	11-06-2013	967	
258	Pedestal	11-06-2013	11-06-2013	4	
259	Cosmics	11-06-2013	14-06-2013	2149	
260	Pedestal	14-06-2013	14-06-2013	4	
261	Cosmics	14-06-2013	24-06-2013	7961	
262	Pedestal	24-06-2013	24-06-2013	4	New chip settings loaded (Settings 8).
263	Cosmics	24-06-2013	27-06-2013	2233	
264	Pedestal	27-06-2013	27-06-2013	3	
265	Cosmics	27-06-2013	09-07-2013	9084	
266	Pedestal	09-07-2013	09-07-2013	6	
267	Cosmics	09-07-2013	10-07-2013	820	

Table A.1: Data overview

Run	**Mode**	**Start date**	**Stop date**	**Triggers**	**Details**
268	Cosmics	10-07-2013	12-07-2013	1430	
269	Pedestal	12-07-2013	12-07-2013	4	
270	Cosmics	12-07-2013	15-07-2013	2129	
271	Pedestal	15-07-2013	15-07-2013	4	
272	Cosmics	15-07-2013	16-07-2013	757	
273	Pedestal	16-07-2013	16-07-2013	4	
274	Cosmics	16-07-2013	18-07-2013	1604	
275	Pedestal	18-07-2013	18-072013	4	
276	Cosmics	18-07-2013	22-07-2013	35	A crash occurred during measurement.
277	Pedestal	22-07-2013	22-07-2013	4	
278	Cosmics	22-07-2013	25-07-2013	2240	
279	Pedestal	25-07-2013	25-07-2013	4	
280	Cosmics	25-07-2013	25-07-2013	191	
281	Cosmics	25-07-2013	30-07-2013	2081	

Appendix B

Chip settings overview

Table B.1: Settings 1 (used from 04-02-2013 to 25-03-2013).

Settings 1 (used from 04-02-2013 to 25-03-2013)								
Slot	Port 1		Port 2		Port 3		Port 4	
#	*P1*	*P2*	*P1*	*P2*	*P1*	*P2*	*P1*	*P2*
1	70	80	120	80	145	80	143	80
2	150	80	140	80	130	80	120	80
3	170	80	160	80	130	80	155	80
4	170	80	155	80	147	80	155	80
5	110	80	230	80	170	80	140	80
6	170	80	150	80	145	80	165	80
7	155	80	159	80	150	80	175	80
8	135	80	170	80	135	80	110	80
9	130	80	205	80	130	80	185	80
10	140	80	165	80	160	80	145	80
11	155	80	110	80	135	80	138	80
12	120	80	125	80	120	80	145	80
1	130	80	125	80	170	80	40	80
2	190	80	130	80	150	80	133	80
3	160	80	160	80	145	80	155	80
4	137	80	220	80	115	80	70	80
5	120	80	130	80	245	80	65	80
6	170	80	205	80	150	80	155	80
7	150	80	155	80	50	80	95	80
8	135	80	190	80	175	80	100	80
9	130	80	153	80	175	80	110	80
10	158	80	160	80	160	80	140	80
11	152	80	155	80	160	80	145	80
12	75	80	175	80	135	80	120	80

Table B.2: Settings 2 (used from 25-03-2013 to 11-04-2013).

Settings 2 (used from 25-03-2013 to 11-04-2013)								
Slot	Port 1		Port 2		Port 3		Port 4	
#	*P1*	*P2*	*P1*	*P2*	*P1*	*P2*	*P1*	*P2*
1	60	80	110	80	135	80	133	80
2	140	80	130	80	120	80	110	80
3	160	80	150	80	120	80	145	80
4	160	80	145	80	137	80	145	80
5	100	80	220	80	160	80	130	80
6	160	80	140	80	135	80	155	80
7	145	80	149	80	140	80	165	80
8	125	80	160	80	125	80	100	80
9	120	80	195	80	120	80	175	80
10	130	80	155	80	150	80	1345	80
11	145	80	100	80	125	80	128	80
12	110	80	115	80	110	80	135	80
1	120	80	115	80	160	80	30	80
2	180	80	120	80	140	80	123	80
3	170	80	150	80	135	80	145	80
4	127	80	210	80	105	80	60	80
5	110	80	120	80	235	80	55	80
6	160	80	195	80	140	80	145	80
7	140	80	145	80	60	80	85	80
8	125	80	180	80	165	80	90	80
9	120	80	143	80	165	80	100	80
10	148	80	150	80	150	80	130	80
11	142	80	145	80	150	80	135	80
12	65	80	165	80	125	80	110	80

Table B.3: Settings 3 (used from 11-03-2013 to 22-04-2013).

Settings 3 (used from 11-03-2013 to 22-04-2013)								
Slot	Port 1		Port 2		Port 3		Port 4	
#	*P1*	*P2*	*P1*	*P2*	*P1*	*P2*	*P1*	*P2*
1	80	80	120	80	145	80	143	80
2	130	80	100	80	130	80	120	80
3	150	80	160	80	130	80	155	80
4	170	80	135	80	147	80	155	80
5	110	80	110	80	160	80	140	80
6	170	80	140	80	145	80	145	80
7	155	80	80	80	150	80	175	80
8	135	80	135	80	135	80	110	80
9	130	80	145	80	120	80	185	80
10	140	80	165	80	160	80	145	80
11	145	80	95	80	135	80	138	80
12	100	80	125	80	100	80	120	80
1	130	80	125	80	170	80	90	80
2	190	80	110	80	145	80	130	80
3	145	80	160	80	145	80	150	80
4	137	80	230	80	115	80	80	80
5	80	80	130	80	240	80	80	80
6	155	80	205	80	110	80	135	80
7	150	80	155	80	80	80	95	80
8	80	80	230	80	155	80	80	80
9	105	80	125	80	175	80	95	80
10	158	80	150	80	160	80	140	80
11	150	80	155	80	150	80	145	80
12	80	80	175	80	130	80	100	80

Table B.4: Settings 4 (used from 22-03-2013 to 06-05-2013)

Settings 4 (used from 22-03-2013 to 06-05-2013)								
Slot	Port 1		Port 2		Port 3		Port 4	
#	*P1*	*P2*	*P1*	*P2*	*P1*	*P2*	*P1*	*P2*
1	80	80	120	80	145	80	143	80
2	140	80	90	80	130	80	125	80
3	160	80	155	80	130	80	145	80
4	165	80	145	80	150	80	160	80
5	95	80	80	80	165	80	150	80
6	175	80	145	80	150	80	155	80
7	145	80	80	80	160	80	165	80
8	145	80	145	80	130	80	115	80
9	120	80	145	80	120	80	195	80
10	144	80	160	80	150	80	155	80
11	150	80	85	80	125	80	143	80
12	95	80	120	80	90	80	125	80
1	125	80	130	80	175	80	80	80
2	195	80	105	80	145	80	120	80
3	135	80	165	80	135	80	145	80
4	130	80	220	80	110	80	80	80
5	80	80	135	80	255	80	80	80
6	165	80	210	80	115	80	145	80
7	145	80	162	80	80	80	85	80
8	80	80	250	80	135	80	90	80
9	90	80	130	80	170	80	85	80
10	167	80	170	80	165	80	145	80
11	142	80	160	80	150	80	155	80
12	80	80	180	80	130	80	90	80

Table B.5: Settings 5 (used from 06-05-2013 to 16-05-2013).

Settings 5 (used from 06-05-2013 to 16-05-2013)								
Slot	Port 1		Port 2		Port 3		Port 4	
#	*P1*	*P2*	*P1*	*P2*	*P1*	*P2*	*P1*	*P2*
1	90	80	120	80	150	80	153	80
2	130	80	110	80	130	80	120	80
3	160	80	155	80	120	80	165	80
4	165	80	140	80	155	80	150	80
5	105	80	90	80	155	80	140	80
6	180	80	140	80	150	80	165	80
7	150	80	80	80	150	80	180	80
8	135	80	140	80	130	80	110	80
9	135	80	105	80	140	80	185	80
10	144	80	170	80	170	80	145	80
11	160	80	100	80	120	80	143	80
12	110	80	130	80	80	80	130	80
1	125	80	120	80	165	80	80	80
2	185	80	120	80	150	80	140	80
3	130	80	160	80	155	80	155	80
4	140	80	240	80	125	80	80	80
5	80	80	135	80	250	80	80	80
6	160	80	215	80	115	80	165	80
7	160	80	155	80	80	80	105	80
8	80	80	250	80	115	80	90	80
9	120	80	140	80	175	80	105	80
10	160	80	160	80	170	80	150	80
11	162	80	160	80	155	80	150	80
12	80	80	180	80	125	80	110	80

Table B.6: Settings 6 (used from 16-05-2013 to 31-05-2013).

Settings 6 (used from 16-05-2013 to 31-05-2013)								
Slot	Port 1		Port 2		Port 3		Port 4	
#	*P1*	*P2*	*P1*	*P2*	*P1*	*P2*	*P1*	*P2*
1	60	80	100	80	125	80	130	80
2	140	80	100	80	130	80	100	80
3	160	80	155	80	115	80	155	80
4	160	80	150	80	147	80	150	80
5	110	80	170	80	140	80	130	80
6	170	80	135	80	140	80	155	80
7	155	80	100	80	135	80	170	80
8	130	80	145	80	135	80	110	80
9	130	80	155	80	120	80	170	80
10	130	80	165	80	160	80	140	80
11	155	80	105	80	130	80	135	80
12	105	80	110	80	110	80	130	80
1	115	80	125	80	165	80	90	80
2	180	80	110	80	140	80	130	80
3	145	80	140	80	145	80	145	80
4	130	80	220	80	110	80	100	80
5	80	80	120	80	240	80	118	80
6	150	80	200	80	110	80	140	80
7	150	80	140	80	100	80	95	80
8	120	80	190	80	165	80	100	80
9	110	80	135	80	170	80	100	80
10	150	80	140	80	150	80	140	80
11	152	80	150	80	150	80	140	80
12	100	80	170	80	130	80	110	80

Table B.7: Settings 7 (used from 31-05-2013 to 24-06-2013).

Settings 7 (used from 31-05-2013 to 24-06-2013)								
Slot	Port 1		Port 2		Port 3		Port 4	
#	*P1*	*P2*	*P1*	*P2*	*P1*	*P2*	*P1*	*P2*
1	70	80	120	80	145	80	143	80
2	150	80	140	80	130	80	120	80
3	170	80	160	80	130	80	155	80
4	170	80	155	80	147	80	155	80
5	110	80	230	80	170	80	140	80
6	170	80	150	80	145	80	165	80
7	155	80	159	80	150	80	175	80
8	135	80	170	80	135	80	110	80
9	130	80	205	80	130	80	185	80
10	140	80	165	80	160	80	145	80
11	155	80	110	80	135	80	138	80
12	120	80	125	80	120	80	145	80
1	130	80	125	80	170	80	40	80
2	190	80	130	80	150	80	133	80
3	160	80	160	80	145	80	155	80
4	137	80	220	80	115	80	70	80
5	120	80	130	80	245	80	65	80
6	170	80	205	80	150	80	155	80
7	150	80	155	80	50	80	95	80
8	135	80	190	80	175	80	100	80
9	130	80	153	80	175	80	110	80
10	158	80	160	80	160	80	140	80
11	152	80	155	80	160	80	145	80
12	75	80	175	80	135	80	120	80

Table B.8: Settings 8 (used from 24-06-2013 to 30-07-2013).

Settings 8 (used from 24-06-2013 to 30-07-2013)								
Slot	Port 1		Port 2		Port 3		Port 4	
#	*P1*	*P2*	*P1*	*P2*	*P1*	*P2*	*P1*	*P2*
1	60	80	110	80	135	80	143	80
2	140	80	130	80	130	80	110	80
3	160	80	160	80	120	80	155	80
4	165	80	145	80	150	80	155	80
5	110	80	90	80	155	80	140	80
6	180	80	140	80	150	80	155	80
7	155	80	159	80	150	80	175	80
8	135	80	145	80	135	80	100	80
9	135	80	205	80	120	80	185	80
10	144	80	160	80	160	80	145	80
11	150	80	100	80	125	80	138	80
12	110	80	120	80	90	80	135	80
1	125	80	125	80	170	80	40	80
2	185	80	120	80	150	80	130	80
3	130	80	160	80	145	80	155	80
4	127	80	220	80	105	80	80	80
5	120	80	120	80	250	80	80	80
6	160	80	205	80	110	80	145	80
7	150	80	155	80	50	80	95	80
8	135	80	190	80	165	80	90	80
9	120	80	130	80	175	80	95	80
10	160	80	170	80	160	80	130	80
11	152	80	155	80	150	80	145	80
12	65	80	175	80	125	80	110	80